Exploratory simulations of multiscale effects of deformation twinning on the mechanical behavior of FCC and HCP metals

Robert Allen

Exploratory simulations of multiscale effects of deformation twinning on the mechanical behavior of FCC and HCP metals

By

Robert Allen

A Dissertation
Submitted to the Faculty of
Mississippi State University
in Partial Fulfillment of the Requirements
for the Degree of Doctorate of Science
in Physics of Materials Science
in the Ecole Doctoral

Mississippi State, Mississippi

July 2018

Exploratory simulations of multiscale effects of deformation twinning

on the mechanical behavior of FCC and HCP metals

By

Robert Allen

Approved:

Laszlo Toth
(Major Professor)

Tamas Ungar
(Rapporteur)

Satyam Suwas
(Rapporteur)

Haitham El Kadiri
(Jury Member)

Andrew Oppedal
(Jury Member)

Somjeet Biswas
(Jury Member)

Roxane Massion
(Jury Member)

Luis Barrales-Mora
(Jury Member)

Laurent Capolungo
(Invited Jury Member)

Name: Robert Allen

Date of Degree: July 26, 2018

Institution: Université de Lorraine and Mississippi State University

Major Field: Physics of Materials Science

Major Professor: Laszlo Toth

Title of Study: Exploratory simulations of multiscale effects of deformation twinning on the mechanical behavior of FCC and HCP metals

Pages of Study: 115

Candidate for Degree of Doctorate of Science

Methods designed for incorporation into multiscale modeling polycrystals are presented in this work in two tasks. This work contains mesoscale methods for capturing the effects of both the interactions of slip dislocations encountering twin grain boundaries and the simultaneous growth of multiple twin grain volume fractions on mechanical hardening and texture evolution. These are implemented in a crystal plasticity framework using the Los Alamos visco-plastic self consistent code, VPSC-7.

Presented here, the effects of simultaneous growth in multiple twin variants on textural evolution is tracked using a Kalidindi-type twin volume transfer scheme. In Task 1, the implementation of this scheme in order to simulate the texture of Twinning Induced Plasticity steels (TWIP) subjected to Equal Channel Angular Pressing (ECAP) are summarized.

In Task 2, the hardening effects of two types of interactions between slip dislocations and encountered twin grain boundaries, namely dislocation transmutation and dissociation, are captured by way of modifying the dislocation density based hardening model of

[11]. Interactions of the first type are presented in a constitutive relation calculating the amount of dislocation density apportioned to a given slip system contained within the encountered twin volume fraction from each interacting slip system in the parent volume fraction. The amount transmuted from each interacting slip system described using the Correspondence Method, an onto mapping of slip systems in a parent grain to slip systems in considered twin grains. Interactions of the second type are then introduced into this constitutive relation as a disassociation parameter, the value of which is established by observations gleaned from the results of the molecular dynamics simulations of [8] and [53]. These methods are implanted to simulate the anisotropic hardening behavior of HCP magnesium under multiple load paths.

Les méthodes conçues pour être incorporées dans des polycristaux de modélisation multi-échelles sont présentées dans ce travail en deux tâches. Ce travail contient des méthodes à moyenne échelle pour capturer les effets des interactions de dislocations de glissement rencontrant des joints de grains maclage et la croissance simultanée de plusieurs fractions de volume de grains maclage sur le durcissement mécanique et l'évolution de la texture. Celles-ci sont mises en uvre dans un cadre de plasticité cristalline utilisant le code visco-plastic self consistent de Los Alamos, VPSC-7.

Présentés ici, les effets de la croissance simultanée de multiples variantes maclage sur l'évolution de la texture sont suivis à l'aide d'un schéma de transfert de volume double de type Kalidindi. Dans la tâche 1, la mise en uvre de ce schéma afin de simuler la texture des aciers à plasticité induite par maclage (TWIP) soumis au pressage angulaire à canal égal (ECAP) est résumée.

Dans la tâche 2, les effets de durcissement de deux types dinteraction entre les dislocations de glissement et les joints de grain maclage rencontrés, à savoir la transmutation et la dissociation de dislocation, sont capturés au moyen de la modification du modèle de durcissement basé sur la densité de dislocation de [11]. Les interactions du premier type sont présentées dans une relation constitutive calculant la quantité de densité de dislocations attribuée à un système de glissement donné contenu dans la fraction de volume maclage rencontrée à partir de chaque système de glissement en interaction dans la fraction de volume mère. La quantité transmutée à partir de chaque système de glissement en interaction décrit à laide de la méthode de correspondance, sur la cartographie des systèmes de glissement dun grain parent à des systèmes de glissement dans des grains maclage considérés. Des interactions du second type sont ensuite introduites dans cette relation constitutive en tant que paramètre de dissociation, dont la valeur est établie par les observations tirées des résultats des simulations de dynamique moléculaire de [8] et [53]. Ces méthodes sont implantées pour simuler le comportement de durcissement anisotrope du magnésium HCP sous plusieurs chemins de charge.

Key words: Twinning, Magnesium, TWIP, dislocation, crystal plasticity, VPSC, SPD, ECAP

DEDICATION

To Finnley, Sarah, Luke, Margot, and the rest of my family.

ACKNOWLEDGEMENTS

The research presented herein was sponsored by LabEX DAMAS as part of Université de Lorraine, by the Chateaubriand Fellowship of the Office for Science & Technology of the Embassy of France in the United States, and by the Army Research Laboratory under Cooperative Agreement NumberW911NF-15-2-0025. The views and conclusions contained in this document are those of the authors and should not be interpreted as representing the official policies, either expressed or implied, of the Army Research Laboratory or the U.S. Government. The U.S. Government is authorized to reproduce and distribute reprints for Government purposes notwithstanding any copyright notation herein.

Additionally, the author would like to acknowledge the guidance and support of Dr. Haitham El Kadiri, Dr. Laszlo Toth, Dr. Andrew Oppedal, Dr. Edward Luke, and Dr. Hyeona Lim over the course of this research.

TABLE OF CONTENTS

LIST OF TABLES

LIST OF FIGURES

LIST OF SYMBOLS, ABBREVIATIONS, AND NOMENCLATURE

DMREF Designing Materials to Revolutionize and Engineer our Future

MGI Materials Genome Initiative for Global Competitiveness

RVE Representative Volume Element

FEA Finite Element Analysis

FD Finite Difference (methods)

TWIP TWinning Induced Plasticity (steel)

TRIP TRansformation Induced Plasticity (steel)

SFE Stacking Fault Energy

ECAE Equal Channel Angular Extrusion

FECP Finite Element Crystal Plasticity

FFT Fast Fourier Transform

CRSS Critical Resovled Shear Stress

SC Self-Consistent (methods)

VPSC Viscoplasitc Self-Consistent

FCC Face Centered Cubic

HCP Hexagonal Close Packed

MTS Mechanical Threshold Stress

CG Composite Grain

VFT Volume Fraction Transfer

PTR Predominate Twin Reorientation (scheme)

PTS Predominate Twin System

ISV Internal State Variable

TVT Twin Volume Transfer

HP Hall-Petch

CHAPTER I

INTRODUCTION

The advancement of scientific, economic, and military competitiveness is driven by continued technological development. Continued development of new technologies is predicated upon the discovery and deployment of new material systems, designed to meet contemporary and future engineering demands. Supported by the *National Science Foundation* through the auspices of *Designing Materials to Revolutionize and Engineer our Future* (DMREF) program, the *Materials Genome Initiative for Global Competitiveness* (MGI) aims to reduce the current development time for new material systems from a range of 10 to 20 years from discovery to deployment, to 2 to 3 years [103, 107]. To this end, coordination and funding efforts have been focused on researching and developing accurate computational material models implemented via well documented, open platform software for general use in science and engineering. These models and their resulting simulation will be stored in and accessed by way of a unified materials database available to the community as part of the MGI [103].

1.1 Role of Computational Methods in the Materials Genome Initiative for Global Competitiveness

Established in 2011, the MGI aims to dramatically reduce the time to take new material systems from the beginning of the discovery and design phases to the first phase of implementation by fifty percent or more. The success of the MGI is predicated on the integration of three pillars of action; these pillars are the greater development and implentation of computational methods for simulating materials systems, newly updated, more transparent and properly currated material data, and greater integration of physically based methods for prototyping and design with available computational tools.

State of the art computational methods are based on multiscale approaches that consider the effect of various phenomena occuring across a variety of length scales on overall mechanical behavior. In this approach, data gleaned from atomistic and molecular dynamics simulations are fed to models for material behavior at a microstructural level to inform processes like texture evolution, dislocation movement and interaction, grain boundary migration, chemical processes like diffusion, and even void growth due to damage or fission reactions. This information is, in turn, used to calculate moduli for stress and strain relations at the continuum level to simulate bulk material behavior of a representative volume element (RVE) of the considered material. RVEs can then be taken as the basis for component level simulations by implementing them as part of macroscale methods like Finite Elemement Analysis (FEA), Finite Difference (FD) methods , or other general approaches. Pairing the correct methods to describe a material at each length scale is of paramount importance.

At every length scale, these models rely on complete data sets for calibration, verification, and validation in order to accurately predict material behavior. In order to advance the

first pillar of greater development of computational methods, the MGI seeks to establish a standardization of practices for the sharing of predicitive algorithms and computational methods and advance the capacity of researchers to exchange and currate material data from physical experiments in order to better calibrate their models.

1.2 Twinning Polycrystals: TWIP Steel and Magnesium

Most plastic deformation in crystalline solids is achieved through crystallographic slip. This process is facilitated by the glide of dislocations across corresponding crystallographic glide planes, and the number and nature of the dislocations present play an important role in plastic deformation. Dislocations may interact with both other dislocations and grain boundaries of a polycrystal. Dislocations may repel, attract, or annihilate each other upon contact, thereby affecting the development of stress in the solid. Additionally they may either pass through or pile up at grain boundaries, and such behavior may inhibit the plastic deformation of a polycrystal by what is known as the Hall-Petch phenomena [45, 85].

In crystalline solids, mechanical twinning is the reorientation of portions of the crystal lattice in order to accommodate strain. Shear strain results in a uniform reorientation of the twinned region that produces a new lattice structure mirroring the original lattice across a plane of shear, and dramatically alters the polycrystal texture of the solid [14].

These processes do not occur independent from one another, and so improvement of the techniques used in predictive modeling for polycrystalline materials depends on a com-

prehensive understanding of the interactions between slip and twinning. In magnesium and magnesium alloys, dislocations may interact with twin grain boundaries. In some cases, dislocations may transmute across twin boundaries to harden the twin grain, and in other cases they may dissociate into twinning disconnections that move twin boundary, thereby increasing the volume fraction of the twin [53]. In other materials, such as TWinning Induced Plasticity (TWIP) steels, dislocations are thought to disassociate into disconnections that pile up and harden twin boundaries in what is know as the Basinski effect [9]. The ability to effectively and accurately bridge the gaps between the behavior at the atomistic scale of dislocations to the single crystal level, and from the single crystal level to a polycrystal continuous medium is what will determine the limits of understanding of polycrystalline material behavior.

1.2.1 Twinning Induced Plasticity Steel

TWIP steels are a class austenitic steels characterized by low stacking fault energy (SFE) and high mangenese content, both of which contribute to a relatively high incidence of mechanical twinning. In more commonly encoutered strain regimes, total twin volume fraction can be as high as 20% of the overall volume, and the twin volume fraction can grow to be nearly 80% in the strain regimes encountered in severe plastic deformation [102]. The formation of twins in the microstructure of TWIP steels is associated with high work hardening rate which leads them to exhibit high strength and ductility with observed yield stress of approximately 1000 MPa and an elongation at failure of approximately 60% under tensile loading [5].

TEM and EBSD imaging of Fe-Mn-C TWIP steel subjected to up to 50% tensile strain has shown the nucleation of bundles or stacks of flat twin grains inside TWIP steel parent grains. Twin grain thickness is typically observed to be between 10 nm and 40 nm [2, 5, 17]. Experiments in TWIP steel during up to four equal channel angular extrusion (ECAE) passes observed similar twin structures even in shear strains of up to 1000% [42]. This suggests that the growth of overall twin volume fraction is motivated by the nucleation of new twin grains rather than the growth of existing twins.

The significant variation of lattice orientation of the parent grain in the neighborhood of twin boundaries not reported in the interior of twin grains suggest dislocation pile-up at twin boundaries [5, 17]. Consequently, twin grains are considered to be relatively rigid compared to their surrounding parent volumes, and are typically considered to be between 2 and 10 times harder in material simulations [24]. That their boundaries are considered to act as barriers to dislocation movement demonstrates that much of the work hardening behavior in TWIP steel can be attributed to Hall-Petch mechanisms[102, 2, 5, 17]. Given this and the unique nature of nucleation dominated twin growth in TWIP steels, the geometry of the twin grains plays and important role in its mechanical behavior.

1.2.2 Magnesium

Magnesium is a hexagonal close-packed crystalline material whose microstructural evolution under deformation is characterized by a high incidence of twinning. In some cases, twin volume fraction approaches 80%-100% of overall volume fraction at as little as 10% strain. Its lightweight and owing to its low density has made magnesium and its

alloys materials of particular interest in the search for improved materials for component design. Even so, magnesium is prone to brittle failure, limiting its use.

Although both the $<1\ 0\ \bar{1}\ 2>$ tensile twinning mode and $<1\ 0\ \bar{1}\ 1>$ compressive twinning mode exist in magnesium, tensile twinning is observed to be highly favored in the formation of twin volume fraction. In both cases, the presence of both twin modes are associated with the formation of cracks. In the case of tensile twins, voids are observed at points of intersections between twin planes. In the case of compressive twins cracks are observed to form along twin boundaries. For this reason, any understanding of the broader behavior of magnesium is predicated on understanding the behavior of the material along twin grain boundaries.

Given the amount of twinning observed in magnesium, much of the simulation work performed on it assumed that Hall-Petch effects would provide siginificant contributions to its hardening evolution. The molecular dynamics simulations of Barrett and El Kadiri [8, 53] observed basal slip dislocations encountering tensile twin boundaries exhibiting behaviors different from the Hall-Petch type interactions seen in twin boundary/dislocation interaction in TWIP steels. In these simulations, screw type dislocations were seen to dissociate when encountering twin boundaries rather than build up as would be the case with Hall-Petch effects. Edge type dislocations exhibited differing behaviors depending on their orientation relative to the twin grain boundary itself. In some cases, they dissociated at the twin grain boundary while emitting twinning disconnections that contribute to twin boundary migration. In other cases, edge dislocations in the parent grain volume were seen to effectively transmute across twin grain boundaries, generating similar dislocations

on different crystalographic planes inside the twin volume [8]. The variety of types of observed slip/twin interactions suggests that phenomena outside of Hall-Petch mechanisms may have a profound effect on the material behavior of magnesium

1.3 Simulation Methods for Polycrystals: An Overview

As research in materials science continues, computational modeling and simulation will play an increasing role in reducing the development cycle of new material systems. A variety of crystal plasticity based approaches have been developed for both single crystal simulations and simulations designed to capture the interaction of polycrystal materials. These approaches primarily differ in the way that they treat the problem of relating the behavior of grains with a single crystal orientation to the behavior of the entire polycrystal aggregate.

The Self Consistent methods utilize micromechanics to approximate the behavior of each grain relative to an averaged polycrystal by treating as an inclusion problem. The stress and strain concentration tensors for each grain may be calculated and an effective polycrystal modulus can be found for each strain increment in this way. The limitations of this method are that grain geometry must be approximated in the course of micromechanical formulation. Therefore, great care must be taken in order to insure physical admissibility of obtained results.

Finite Element Crystal Plasticity (FECP) directly models the stress and strain fields of polycrystals by recreating the polycrystal geometry directly. This method uses finite

element meshes of sufficient resolution to allow for greater precision in capturing the geometry of the polycrystal contained in a representative volume element. Computational costs, however, limit the number of grains and the complexity of their geometry. This represents the primary limitation of this method. More recently, a method of using fast Fourier transforms (FFT) has been used to solve for the averaged stress and strain fields within a representative volume element (RVE). While this method has yielded gains in speed, it is limited in its applicability to polycrystals with a periodic structure.

Taking all of these methods into consideration, it is apparent that the continued development of multi-scale modeling approaches that capture the effects of lower length scale behaviors on continuum level behavior will pave the way for a greater understanding of the complex interactions at work in these materials and aid in the development of new designs based there on.

1.4 Research Goals and Project Overview

The aim of this work is to examine the roles played by twinning driven textural development and dislocation interactions with twin grain boundaries in the continuum level mechanical behavior of polycrystal magnesium and TWIP steels. This examination is to be carried about by the development and utilization of a new, multi-scale, crystal plasticity based modeling scheme to be implemented in a modified VPSC micro-mechanical framework. This is done with the intent to answer the following research questions:

1. To what extent does the simultaneous inclusion of the contributions of multiple twin systems to textural evolution affect the ability to simulate and predict texture evo-

lution in twinning polycrystals? Can these methods be used to supplement current approaches utilizing twin variant selection?

2. Does dislocation transmutation motivate hardening behavior in heavily twinning materials? If so, to what extent? Is there sufficient evidence to suspect that twin grain hardness due to transmutation effects acts as the primary driver of polycrystal materials in which it occurs or does it supplement Hall-Petch driven hardening?

3. What steps might be employed that reduce the reliance on empirically based methods used to "fit" modeling data to pre-existing data?

1.4.1 Research Design

While previous works have made great strides in modeling and simulating of the mechanical behavior of polycrystal metals, there are still significant tasks that remain. In order to advance the goals of this work, two shortfalls are addressed:

1. The current spread of twin growth schemes do not currently include physically based schemes of sufficient generality to be applied to the range of twin morphologies seen in both TWIP steels and magnesium and magnesium alloys while capturing the associated textural developments.

2. A truly multiscale treatment of polycrystal deformation should be able to recreate the stress and strain responses of each material while including physically motivated descriptions of the behavior at the scales of both grains and dislocations. To do this, twin growth needs to be coupled with the processes found at the dislocation scale in a physically meaningful sense. The list of dislocation scale processes should include dislocation interactions with grain boundaries, both in terms of transmutation and dissociation into twinning disconnections. To date, such a scheme treatment does not exist.

These three shortfalls represent the direction of effort of the work proposed herein. In turn, the proposed work may be subdivided into three distinct tasks in order to better address the aforementioned shortfalls in modeling and simulation technology. These are

1. In order to inject more phenomenological motivation into the method of simulating twin volume growth, the volume transfer scheme of [36] will be modified to include twin volume growth attenuation as a function of each twin grain's deviation from it's ideal orientation relative to its parent, and implemented in the code of VPSC-7d.

This model for twinning will be tested on TWIP steels deformed by ECAP before being applied to pure magnesium.

2. In order to capture the interaction of dislocations with twin grain boundaries, the dislocation transmutation scheme of [55] will be adapted and implemented in VPSC and applied to pure magnesium.

CHAPTER II

LITERATURE REVIEW

Broadly speaking, the aim of this work is to provide a novel approach to modeling the behavior of twinning polycrystals that is both comprehensive and physically motivated. What follows in this chapter is a summary of previous approaches developed to capture the effects of twinning on the polycrystal evolution under mechanical loading. This review is organized first by topic and therein by loose chronological order of development. In an effort to establish and exhaustive theoretical base for the dissertation tasks outlined in the previous chapter, the topics of contextual material characteristics of TWIP steels and magnesium, general single and polycrystal modeling, fundamental concepts of twinning, and modeling approaches for textural evolution and mechanical hardening are reviewed.

2.1 Approaches to Modeling Polycrystals

The modeling of polycrystalline material is complex to say the least, giving due consideration to both intra and inter grain interactions. As a result, a number of methods have been developed, each with its own set of simplifying assumptions postulated in attempts to make the interwoven set of phenoma observed in polycrystal deformation more feasibly simulated. The basis for these approaches lie in the kinematic and kinetic treatments of single, and subsequently, polycrystalline slip.

2.1.1 Crystal Plasticity Framework for Single Crystals

Bridging the gap between continuum and crystal scale is done primarily through the auspices of the modern crystal plasticity mathematical framework. Crystal plasticity for polycrystal modelling and simulation is built on the foundation of single crystal plasticity, where a monocrystal representative volume element that deforms solely by slip is considered. Beginning with this foundation and considering deformation accomodated by the shear glide of a single slip system, the Schmid orientation tensor for single crystal lattice is calculated as

$$\mathbf{m} = \mathbf{bn} \tag{2.1a}$$

$$m_{ij} = b_i n_j \tag{2.1b}$$

Here, the vectors **b** and **n** are the Burger's vector and the vector normal to the plane of slip. Using the Schmid tensor, the velocity gradiant may be composed from the shear strain rate of of the considered slip system as

$$L_{ij} = m_{ij}\dot{\gamma} \tag{2.2}$$

For the case of the deformation of a single crystal with multiple slip systems s, the total strain rate for the crystal can be described as the summation of shear deformation on each system as

$$\dot{\epsilon}_{ij} = \sum_{s=1}^{N} \frac{1}{2}\left(m_{ij}^{s} + m_{ji}^{s}\right)\dot{\gamma}^{s} \tag{2.3}$$

Given an imposed velocity gradiant at the level of the RVE, the individual contributions remain unknown without additional constraints. The various crystal plasticity constraints

all begin with the representation of the 2^{nd} order strain rate tensor as a five element vector through the relation

$$\dot{\epsilon} = (\dot{\epsilon}_1, \dot{\epsilon}_2, \dot{\epsilon}_3, \dot{\epsilon}_4, \dot{\epsilon}_5) = \left(\frac{(\dot{\epsilon}_{22} - \dot{\epsilon}_{11})}{\sqrt{2}}, \frac{\dot{\epsilon}_{33}\sqrt{3}}{\sqrt{2}}, \dot{\epsilon}_{23}\sqrt{2}, \dot{\epsilon}_{31}\sqrt{2}, \dot{\epsilon}_{12}\sqrt{2} \right). \tag{2.4}$$

Similarly, the Schmid tensor component for each slip system may be transformed into a five element vector $\bar{\mathbf{m}}^s$ by

$$\bar{\mathbf{m}}^s = \left(\frac{(m^s_{22} - m^s_{11})}{\sqrt{2}}, \frac{m^s_{33}\sqrt{3}}{\sqrt{2}}, \frac{(m^s_{23} + m^s_{32})}{\sqrt{2}}, \frac{(m^s_{31} + m^s_{13})}{\sqrt{2}}, \frac{(m^s_{12} + m^s_{21})}{\sqrt{2}} \right). \tag{2.5}$$

Therefore the total strain on a polyslip system may be expressed, in this new vector form, as

$$\dot{\epsilon}_i = \sum_{s=1}^{N} \bar{\mathbf{m}}^s_i \dot{\gamma^s}. \tag{2.6}$$

This transformation represents a system of five equations, thereby necissitating five slip systems in order constrain the resulting system of equations sufficiently to reach a solution. However, the number of potential active slip systems exceeds this number considerably, as there are well over 300 unique combinations slip systems to choose from. Consequently, a number of methods for properly constraining the set of equations have been proposed. The works of Taylor, Schmid, and Bishop and Hill all produced methods for ascertaining the number of active slip systems in a deforming RVE. [88, 98, 29, 15] It is, though, the Self Consistent methods which are of greatest interest for the purposes of the proposed work.

The Taylor criterion simply selects the 5 systems for which the summation of slip is minimized. This, however, assumes the existence of a unique minimum set for a given load condition, which is not always the case. This leads to ambiguity in the selection criteria in cases where multiple slip system sets with identical slip sums exist [98]. The

Schmid criterion uses a yield surface based on the **c**ritical **r**esovled **s**hear **s**tress (CRSS) in deviatoric stress space to select the slip systems used to constrain system of equations. The yield surface is described in vectorized form by:

$$\tau^{(s)} = \bar{\mathbf{S}} \cdot \bar{\mathbf{m}}_i^s - \tau_{crit} = 0, \tag{2.7}$$

where $\bar{\mathbf{S}}$ is the 5 dimensional vector representation of the deviatoric stress tensor and τ_{crit} is the critical resolved shear stress. The yield surface, then, is a coomposition of hyperplanes defined by slip systems in the deviatoric stress space. From this definition two kinds of ambiguities arise. In the case of single slip, multiple values of $\tau^{(s)}$ exist at a point on a plane of the yield surface, each associated with the strain rate normal to the plane. As such, the stress state is not unique. At a point of intersection of two planes on the yield surface, only one such $\tau^{(s)}$ exists, but the normality condition for flow is satisfied within a cone bounded by the normal vectors of the two intersecting planes. Consequently, the strain rate normal vector is not unique in this case.

The Bishop-Hill criterion address the ambiguities of the Schmid criterion by introducing a maximum work principle, where the stress states at the set of vertices defined by the intersection of hyperplanes are each calculated. These stress states are then used to calculate work on the slip systems at each of these vertices, the maximum of which are selected for activation. Although this method is useful for reducing the amount of potential active slip systems, it still does not address the strain rate ambiguity left from the definition of yield in the Schmid criterion [15].

A viscoplastic approach can applied to the crystal plasticity framework. In this approach, the strain rate sensivity m for a fixed value ϵ is calculated as:

$$m = \frac{d \ln \sigma}{d \ln \dot{\epsilon}}. \tag{2.8}$$

This rate sensitivity parameter is applied to the kinetic equation for a given slip system s to calculate the resolved shear stress as:

$$\tau_r^s = \tau_0^s \cdot \frac{\dot{\gamma}_r^s}{\dot{\gamma}_0^s} \cdot \mid \frac{\dot{\gamma}_r^s}{\dot{\gamma}_0^s} \mid^{m-1}, \tag{2.9}$$

noting that in order to preserve directionality of shear, the product $\frac{\dot{\gamma}_r^s}{\dot{\gamma}_0^s} \cdot \mid \frac{\dot{\gamma}_r^s}{\dot{\gamma}_0^s} \mid^{m-1}$ is subsituted for $\mid \frac{\dot{\gamma}_r^s}{\dot{\gamma}_0^s} \mid^m$. Solving for the rate of shear $\dot{\gamma}_r^s$ and subsituting the projection of the stress tensor onto the Schmid metric tensor for τ_r^s yields the Hutchinson Strain Rate Law for a single slip system:

$$\dot{\gamma}_r^s = \gamma_0^s \cdot \frac{\bar{S} \cdot \bar{M}}{\tau_0^s} \cdot \mid \frac{\bar{S} \cdot \bar{M}}{\tau_0^s} \mid^n \tag{2.10}$$

where $n = \frac{1}{m} - 1$. This can be summed across multiple slip systems to calcuate total strain rate across a single crystal as:

$$\dot{\epsilon}_i = \gamma_r^0 \sum_{s=1}^{N} M_i^s \cdot \frac{\bar{S} \cdot \bar{M}}{\tau_0^s} \cdot \mid \frac{\bar{S} \cdot \bar{M}}{\tau_0^s} \mid^n \tag{2.11}$$

In vectorized form, this may be expressed as:

$$\dot{\epsilon} = \sum_{s=1}^{N} \bar{\mathbf{m}}_i^s \dot{\gamma^s}. \tag{2.12}$$

As slip rates can be calculated from the rate sensitivity parameter and reference shear rate, the only unknown is the deviatoric stress applied, leading to a final system of five equations and five unknowns.

2.1.2 Approaches to the Modeling of Polycrystals

Extrapolating the behavior of polycrystalline materials from the behavior of their single crystal counterparts is no mean feat, and a variety of approaches have been developed in order to address this issue. These approaches primarily differ in the number and type of simplifying assumptions they make in order to capture specific intergranular phenomena, and how these assumptions dictate the type of numerical methods that might be applied, thereby relating the behavior of grains with a single crystal orientation to the behavior of the entire polycrystal aggregate.

Finite Element Crystal Plasticity (FECP) directly models the stress and strain fields of polycrystals by recreating the polycrystal geometry directly. This method uses finite element meshes of sufficient resolution to allow for greater precision in capturing the geometry of the polycrystal contained in a representative volume element. Computational costs, however, limit the number of grains and the complexity of their geometry. This represents the primary limitation of this method. More recently, a method of using fast Fourier transforms (FFT) has been used to solve for the averaged stress and strain fields within a representative volume element (RVE).

The Self-Consistent (SC) methods utilize micromechanics to approximate the behavior of each grain relative to an averaged polycrystal by treating as an inclusion problem. The limitations of this method are that grain geometry must be approximated in the course of micromechanical formulation. Therefore, great care must be taken in order to insure physical admissibility of obtained results.

Alone, the crystal plasticity framework is insufficient to describe the behavior of polycrystalline materials. This was the primary motivation for the development of Self Consistent Methods. These models were later adapted to include new loading paths in the work of [15]. The treatment of polycrystals changed with the development of micromechanics, introduced by [30] in 1957. Micromechanics utilizes the concept of eigenstrains to construct schemes for the homogenization of mechanical behavior of materials with geometrically complex microstructures. The work of [30] led to the development of the homogenization of elastic polycrystal behavior.

These homogenization techniques were adapted for the simulation of nonlinear mechanical behavior in the works of [21] and [58], and later, the affine linearization approach was developed by [46] as a series of arbitrarily small linear deformation steps meant to approximate nonlinear behavior. Secant and tangent linearizations were later developed in the works of [10] and [76], respectively.

In 1993, the work of [63] adapted the tangent formulation from [76] for the simulation of fully anisotropic materials, including HCP materials. This formed the basis for their Viscoplastic Self-Consistent (VPSC) method and its corresponding code. In this method, the homogeneous polycrystal medium was not assumed to be isotropic, contrasting with other contemporaneous self consistent codes [77]. This approach was expanded by [67] and again in 2000, in the work of [73], to include a generalized affine linearization scheme. The most contemporary form of the VPSC method and code was finally developed in the works of [66].

Beginning by considering the classic inclusion problem of micromechanics, the self-consistent approach of VPSC-7 [101] follows by first defining the linearized stress and strain relationship for a given grain r as

$$\epsilon_{ij}^{r}(\bar{x}) = M_{ijkl}^{r}\sigma_{kl}^{r} + \epsilon_{ij}^{0(r)}. \tag{2.13}$$

Here, M^r and $\epsilon^{0(r)}$ are the viscoplastic compliance tensor and back extrapolated strain for grain r. An analogous relationship between stress and strain of the polycrystal aggregate at the macrolevel is assumed as well, with

$$E_{ij} = \bar{M}_{ijkl}\Sigma_{kl} + E_{ij}^{0} \tag{2.14}$$

In the self-consistent approach, the macrolevel values are assumed to be known *a priori*. These values, however, must still be adjusted self-consistently in accordance with grain level values. In order to do this, the grain level equation needs to be formulated in terms of the macroscopic values and solved. The method for rewriting local grain behavior in terms of macroscopic quantities through the use of an eigenstrain formulation shown in the text of Mura [79] is adopted in VPSC-7 leading to

$$\epsilon_{ij}^{r}(\bar{x}) = \bar{M}_{ijkl}\sigma_{kl}^{r}(\bar{x}) + E_{ij}^{0} + \epsilon_{ij}^{*}(\bar{x}) \tag{2.15}$$

The term ϵ^* in Equation 2.15 is the eigenstrain experienced by the grain resulting from accommodation effects. Letting $\widetilde{\epsilon}$ represent strain fluctuations from macroscopic values inside the grain r, the fluctuations of stress, $\widetilde{\sigma}$, can be computed by combining Equations 2.14 and 2.15 as

$$\widetilde{\sigma}_{ij}(\bar{x}) = \bar{L}_{ijkl}(\widetilde{\epsilon}_{kl}(\bar{x}) - \epsilon_{ij}^{*}(\bar{x})). \tag{2.16}$$

Here, the macroscopic stiffness tensor, $\bar{L} = \bar{M}^{-1}$.

In order to arrive at the final form of the inclusion problem, the compatibility and incompressibility conditions are invoked. Denoting the Cauchy stress tensor and the mean stress as $\widetilde{\sigma}^c$ and $\widetilde{\sigma}^m$, respectively, these conditions are

$$\widetilde{\sigma}^c_{ij,j}(\bar{x}) = \widetilde{\sigma}_{ij,j}(\bar{x}) + \widetilde{\sigma}^m_{,j}(\bar{x}), \tag{2.17}$$

and

$$\widetilde{\epsilon}_{ij} = \frac{1}{2}(\widetilde{u}_{i,j}(\bar{x}) + \widetilde{u}_{j,i}(\bar{x})). \tag{2.18}$$

With some manipulation, the conditions expressed in Equations 2.17 and 2.18 can be utilised with Equation 2.16 to yield the final inclusion problem,

$$\bar{L}_{ijkl}\widetilde{u}_{k,lj}(\bar{x}) + \widetilde{\sigma}^m_{,i}(\bar{x}) + f_i(\bar{x}) = 0, \tag{2.19a}$$

$$\widetilde{u}_{k,k}(\bar{x}) = 0. \tag{2.19b}$$

The term $f(\bar{x})$ represents the fictitious force associated with the heterogeniety of the inclusion and can be expressed in terms of the eigenstrains as

$$f_i(\bar{x}) = -\bar{L}_{ijkl}\epsilon^*_{kl,j}(\bar{x}) = \sigma^*_{ij,j}(\bar{x}). \tag{2.20}$$

The problem in Equations 2.19a and 2.19b is solved using the Green function method in VPSC-7. In this method the solution is obtained by solving an auxiliary problem

$$\bar{L}_{ijkl}G_{km,lj}(\bar{x}) + H_{m,i}(\bar{x}) + \delta_{im}\delta(\bar{x}) = 0, \tag{2.21a}$$

$$G_{km,k}(\bar{x}) = 0. \tag{2.21b}$$

Here, δ and $\delta(\bar{x})$ are the Dirac and Kronecker deltas, repectively. The functions, G and H, are the Green functions associated with $\widetilde{u}$ and $\widetilde{\sigma}^m$ by the convolution integrals

$$\widetilde{u}_k(\bar{x}) = \int_{R^3} G_{ki}(\bar{x} - \bar{x}')f_i(\bar{x}')d\bar{x}', \tag{2.22a}$$

$$\widetilde{\sigma}^m(\bar{x}) = \int_{R^3} H_i(\bar{x} - \bar{x}')f_i(\bar{x}')d\bar{x}'. \tag{2.22b}$$

Applying the Fourier transform method from [65] the velocity deviator for the considered grain can be calculated as

$$\widetilde{u}^r_{k,l}(\bar{x}) = T_{klij}\bar{L}_{ijmn}\epsilon^{*r}_{mn}, \tag{2.23}$$

where the Green interaction tensor, T, is

$$T_{klij} = \frac{abc}{4\pi}\int_0^{2\pi}\int_0^{\pi} \frac{\alpha_j\alpha_l A^{-1}_{ki}(\bar{\alpha})}{[\rho(\bar{\alpha})]^3} sin\theta d\theta d\phi \tag{2.24}$$

In Equation 2.24, θ and ϕ are the spherical coordinates of the Fourier unit vector $\bar{\alpha}$ and the quantities a, b, and c are the ellipsoidal axis of the grain. The quantity A is

$$A_{ik} = \alpha_j\alpha_l\bar{L}ijkl, \tag{2.25}$$

and the function ρ is

$$\rho(\bar{\alpha}) = [(a\alpha_1)^2 + (b\alpha_2)^2 + (c\alpha_3)^2]^{1/2} \tag{2.26}$$

The symmetric and skew-symmetric Eshelby tensors, S and Π can then be constructed from T as

$$S_{ijkl} = \frac{1}{4}(T_{ijmn} + T_{jimn} + T_{ijnm} + T_{jinm})\bar{L}_{mnkl} \tag{2.27a}$$

and

$$\Pi_{ijkl} = \frac{1}{4}(T_{ijmn} - T_{jimn} + T_{ijnm} - T_{jinm})\bar{L}_{mnkl}. \tag{2.27b}$$

The symmetric Eshelby tensor can then be used to compute strain-rate deviations inside of grain r by

$$\widetilde{\epsilon}_{ij}^{r} = S_{ijkl}\epsilon_{kl}^{*r}, \tag{2.28}$$

and the rotation-rate deviations by

$$\widetilde{\omega} = \Pi_{ijkl}\epsilon_{kl}^{*r}. \tag{2.29}$$

Revisiting Equation 2.16 the relation between stress and strain rate fluctuations inside of grain r can then be stated as

$$\widetilde{\epsilon}_{ij}^{r} = -\widetilde{M}_{ijkl}\widetilde{\sigma}_{kl}^{r}, \tag{2.30}$$

where M is

$$\widetilde{M}ijkl = (I - S)_{ijmn}^{-1}S_{mnpq}\bar{M}_{pqkl}. \tag{2.31}$$

Letting the localization tensors B^r and b^r be defined as

$$B_{ijkl}^{r} = (M^r + \widetilde{M})_{ijmn}^{-1}(\bar{M} + \widetilde{M})_{nmkl} \tag{2.32a}$$

and

$$b_{ij}^{r} = (M^r + \widetilde{M})_{ijmn}^{-1}(E_{kl}^{0} - \epsilon_{kl}^{0r}), \tag{2.32b}$$

the stress and strain fields inside grain r can be calculated as functions of macrolevel stress and strain by

$$\sigma_{ij}^{r} = B_{ijkl}^{r}\Sigma_{kl} + b_{ij}^{r} \tag{2.33}$$

and

$$\epsilon_{ij}^{r} = M_{ijkl}^{r}B_{klmn}^{r}\Sigma_{mn} + M_{ijkl}^{r}b_{kl}^{r} + \epsilon_{ij}^{0r}. \tag{2.34}$$

Finally, by defining macroscopic strain as the weighted average of the strain on all grains r, the final polycrystal stress and strain relationship can be self-consistently adjusted as

$$E_{ij} = \langle \epsilon_{ij}^r \rangle = (\langle M^r : B^r \rangle : \angle B^r \rangle)_{ijkl}^{-1} \Sigma_{kl} + \langle (M^r : b^r)_{ij} + \epsilon_{ij}^0 \rangle - \langle M^r : B^r \rangle : \langle B^r \rangle^{-1} : \langle b^r \rangle. \tag{2.35}$$

2.2 Twinning Polycrystals

It is understood that plastic deformation of crystalline solids is often the product of the slip of crystallographic planes across a plane of shear. However, many materials exhibit methods of accommodating such deformation beyond slip. One of these methods is mechanical twinning. Put succintly, mechanical twinning is the reorientation of portions of existing grains, commonly referred to as parent or mother grains, into new orientations, referred to as twin or child grains, defined by a specific angle of misorientation relative to their parent grains that results in a volume preserving homogeneous shear. This reorientation is differentiated from the rigid body rotation observed at the grain level in that rather than simply rotating existing grains into new orientations, twinning results in the formation of entirely new twin grains inside of parent grains. Additionally, multiple twin grains can and often do nucleate and grown inside of a single parent. Consequently, twinning is intimately tied to both the textural and hardening evolution as twinning generates new lattice orientations and twin boundaries can act as barriers to slip dislocation motion.

2.2.1 Kinematic Overview: Correspondence Method

Originally presented in the 1965 work of Bilby [14], the kinematics of twinning are frequently described in terms of a plane of shear, **S**, a twin or composition plane $\mathbf{K}_1$ containing the vector η_1, and the conjugate planes and vectors $\mathbf{K}_2$ containing η_2 for the untwinned lattice that moves to $\mathbf{K}_2'$ containing η_2' in the new twin lattice.

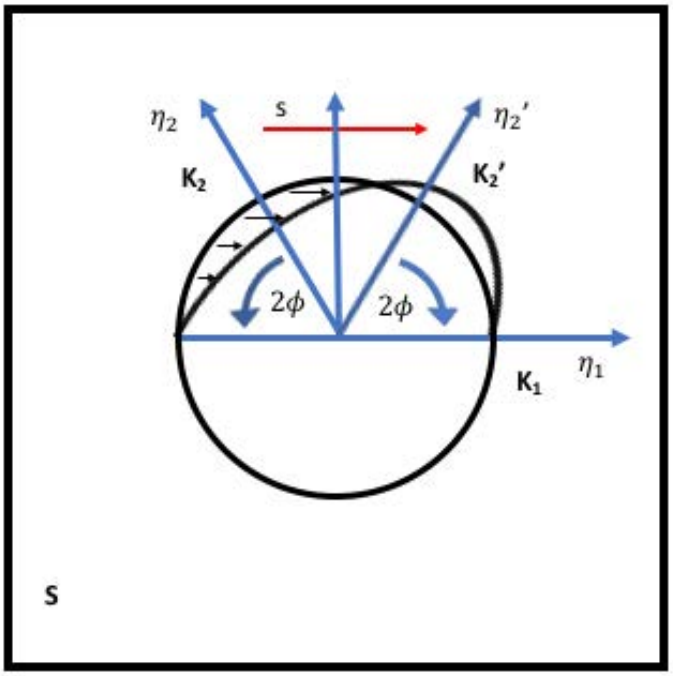

Figure 2.1: Spherical grain element deformed by mechanical twinning presented on the plane of shear **S**.

In the works of Niewczas, this lattice reorientation is described mathematically for Type I mechanical twinning [80, 81]. This was done by first defining a deformation gradient **S**

(not to be confused with the plane of shear from above) composed of a magnitude of twin shear s, a direction of twinning **m**, and the normal to the twin plane **n** by:

$$\mathbf{S} = \begin{bmatrix} 1 + sm_1n_1 & sm_1n_2 & sm_1n_3 \\ sm_2n_1 & 1 + sm_2n_2 & sm_2n_3 \\ sm_3n_1 & sm_3n_2 & 1 + sm_3n_3 \end{bmatrix} \tag{2.36}$$

This deformation gradient may be applied to any vector $\mathbf{u}_M$ described in the orthogonal basis of the parent lattice into a corresponding twinned vector $\mathbf{v}_M$ in the same parent basis as

$$\mathbf{v}_M = \mathbf{S}\mathbf{u}_M \tag{2.37}$$

In order to express the twinned vector $\mathbf{v}_M$ in an orthogonal basis representing the twinned lattice, the twin transformation matrix **X** and rotation about the normal to the twin plane **R** are introduced as

$$\mathbf{X} = \begin{bmatrix} m_1 & m_2 & m_3 \\ m_3n_2 - m_2n_3 & m_1n_3 - m_3n_1 & m_2n_1 - m_1n_2 \\ n_1 & n_2 & n_3 \end{bmatrix} \tag{2.38}$$

and

$$\mathbf{R} = \begin{bmatrix} -1 & 0 & 0 \\ 0 & -1 & 0 \\ 0 & 0 & 1 \end{bmatrix}, \tag{2.39}$$

respectively. Taking $\mathbf{U} = \mathbf{X}^{-1}\mathbf{R}\mathbf{X}$, then any parent lattice vector $\mathbf{u}_M$ transformed into the twin lattice vector $\mathbf{v}_T$ can be related by

$$\mathbf{v}_T = \mathbf{U}\mathbf{S}\mathbf{u}_M. \tag{2.40}$$

In this way, vectors defining the direction and plane of slip in parent grain slip systems can be transformed into their corresponding slip systems inside twinned volume fractions.

2.2.2 Twin Grain Boundary Interactions

The complexity of deformation processes in polycrystal materials is predicated on a number of phenomena. Even when considering only slip, the number of ways in which slip dislocations behave in polycrystals is substantial. Dislocations may initiate and annihilate in response to mechanical and thermal loading, or as a response to interactions between other dislocations. Grain boundaries may migrate with annealing, or facilite sliding of grains past each other. In both cases, dislocations may pile up at grain boundaries resulting in increased hardening refered to as the Hall-Petch mechanism, or may initiate cross-slip, thereby bypassing the grain boundaries. When twinning is considered, the complexity of dislocation interactions and their effects on the mechanical behavior of polycrystal materials can be staggering.

Slip dislocations encountering twin grain boundaries have been observed in experiments and simulations to behave in a number of ways. Molecular dynamics simulations of FCC materials have shown that dislocations may transmute across twin boundaries or they may dissociate or be incorporated into the boundary itself. In other cases they may pile up in a manner consistent with Hall-Petch behavior, and in other cases they may even be emitted on the opposing side of the twin boundary as multiple slip dislocations [31]. Experimentally, dislocations in FFC copper-aluminum alloys have been observed to crossover into advancing twin volume fractions. In this case, dislocations encountering twin grain

boundaries were posited to pile-up at said boundaries. As the twin grain boundary advanced in order to facilitate twin volume growth, these dislocations were overtaken and became sessile dislocations inside the twin volume fraction [9] These finding contrast with the observed behavior of TWIP steels, in which dislocations are seen simple to pile up at twin grain boundaries, thus demonstrating the wide spectrum of behavior even in materials with the same crystal structure [38].

Currently, debate exists regarding the nature of the dislocation-twin grain boundary interactions taking place in deforming magnesium. While nano-indentation studies of twinned magnesium showed no evidence of an increased dislocation density inside of twin volume fraction that would be indicative of dislocation transmutation or Basinski mechanism at work, the observed"gulf" between saturation stress levels of magnesium under different load paths suggests that more hardening mechanisms than simple mechanical anisotropy are at work [48] This has supported the assumption that the evolution of hardening in heavily twinning magnesium is motivated primarily by Hall-Petch effects, with slip dislocations building up at twin grain boundaries [11]. Counter to this assumption, VPSC simulations of rolled magnesium using a twinned storage factor to empirically account for the effects of increased dislocation density inside twin volume fractions were able to successfully recreate the hardening evolution of the material across multiple load paths [55]. The suggestion that dislocation density inside the twinned volume fraction was further supported by molecular dynamics simulations, in which basal dislocations were observed to both transmute across and dissociate to aid the migration of tensile twin boundaries [8, 53].

2.2.3 TWinning Induced Plasticity Steels

Discovered in 1888 by Sir Robert Hadfield, TWIP steels are a type of austenetic FFC steel whose general mechanical behavior combines high yield strength with high elongation (ductility) properties relative to other steels. These traits make TWIP steels highly desirable for implementation in vehicle design and extensive efforts to characterize the material behavior of TWIP steels across a broad range of temperatures, strain rates, and across a spectrum of compositions have been made in the past two decades. Ultimate strength at failure has been observed in the range of 650-1000 MPa with an elongation at failure ranging from 60%-92% [32, 5].

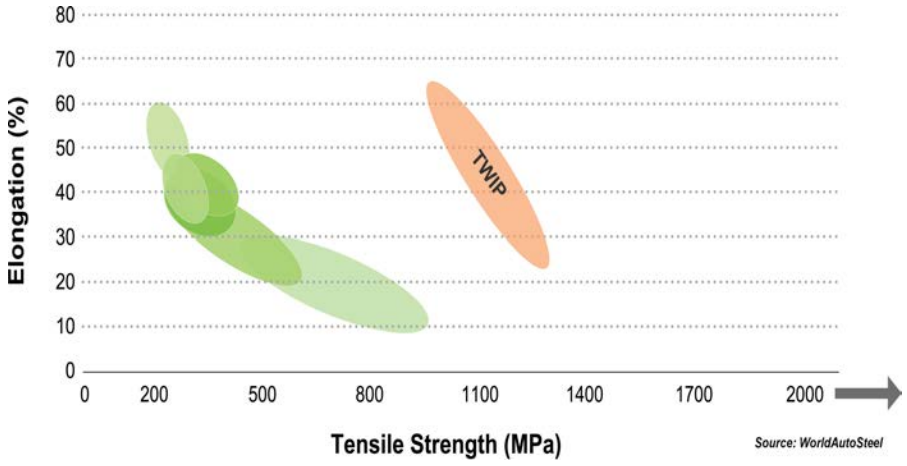

Figure 2.2: The mechanical behaviors of TWIP steels are typically described as operating in a "utopia" region of strength and ductility [108].

The characteristic hardness and ductility of TWIP steels is associated with the incidence of twin nucleation, and is observed to occur preferentially in areas of high deformation. These twin grains exhibit a distinct morphology, which led them to be mischaracter-

ized as shear banding in early studies [2]. Twin grains in TWIP steels nucleate as stacks or bundles of thin twin lamellae. These lamellae are typically observed to be between 30nm and 50nm in thickness [38]

The low observed SFE of TWIP steels is tied primarily to the weighted fraction of Mn content and it is this low SFE of TWIP steels that is associated with plasticity facilitated by both the nucleation of twin volume fractions and martensitic phase transformation in both TWIP and **tr**ansformation **i**nduced **p**lasticity (TRIP) steels, respectively. Other alloyed elements like carbon, silicon, and aluminum have also been observed to play a role in nucleation of twins in TWIP steels, ultimately having an effect on both mechanical strength at failure and elongation [17, 32, 5, 20].

In some studies twin volume fraction has been observed to plateau at approximately 12% of the total volume fraction, even at the large strains seen in severe plastic deformation (SPD) processes [90]. This however has been disputed in other works, where twin volume fractions as high 15% have been observed at strains as low as 0.4. This may be due to the fact that experimental methods for consistenlty and accurately assessing the volume fraction of the micro twins of TWIP steel have yet to be fully realized [17]. Alternately, parent grain size may explain discrepancies in observed twin volume fractions, as grain boundaries have been shown to discourage the nucelation of new twin lamellae, with new twin grains exhibiting a tendancy to form in parent grains of 5 μm diameter or larger [5]. Dislocation pile-up has been observed at the boundaries of these micro-twins and observed slip inside twin volume fractions is relatively scant, consistent with the higher hardness

observed in the twin volume fractions [38]. Consequently, the twin grains are considered quite rigid compared to their parents [24, 95].

2.2.4 Magnesium

Characterized by its light weight, HCP magnesium has been the subject of a resurgence in interest in ongoing efforts to expand its engineering applications. The efforts have been thus far limited by magnesium's poor mechanical performance and low formability relative to other engineering materials [1]. Magnesium exhibits a tendency towards brittle behavior, associated with the presence of high twin volume fractions. Although magnesium's mechanical behavior is highly anisotropic owing to it's crystal structure, observed strength and elongation at failure is typically less than 240 MPa and 20%, respectively [51, 83].

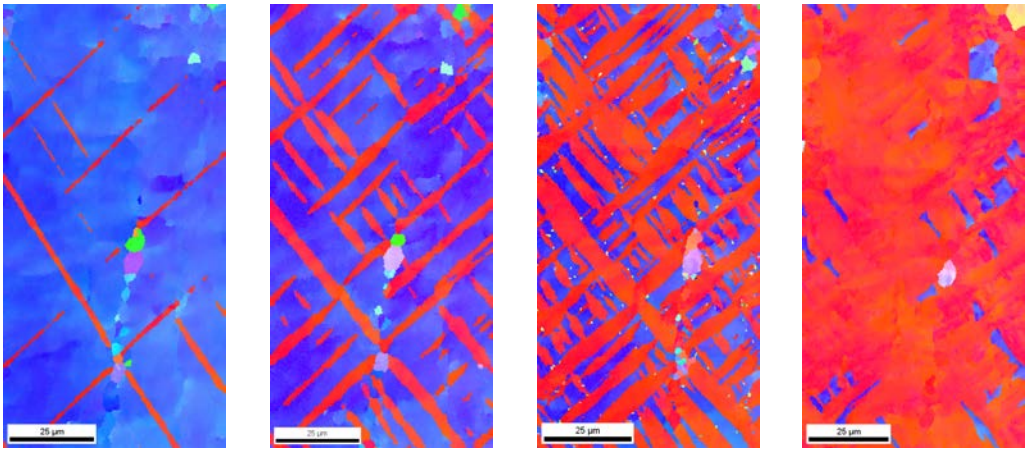

Figure 2.3: EBSD images of twinning magnesium grain from [54] at 2.8%, 3.8%, 6.0%, and 8.0% strain, from left to right.

Magnesium and its alloys possess an HCP crystal structure which gives them an anisotropic behavior at the monocrystal level, resulting in a high load path and texture dependence seen in the mechanical behavior of polycrystal magnesium [82, 13, 22, 47, 28, 26]. The mechanical behavior of magnesium is further complicated by the fact that, for many combinations of texture and loading, slip alone is not sufficient to accommodate deformation, resulting in a high incidence of mechanical twinning. Nucleating primarily along grain boundaries, $\langle 1\,0\,\bar{1}\,2\rangle$ tensile twins have been observed to quickly overtake most of the volume parnet volume fraction, reaching as high as 70% to 90% by strains of 0.2 in specific loading paths [82, 12] Additionally, secondary compressive $\langle 1\,1\,\bar{2}\,2\rangle$ twins have been observed as primary twinning reorients crystal lattices into orientations favorable to such behavior [72, 6] Because twinning in magnesium has been associated with brittle failure a great deal of effort has been put into developing an understanding of the complex interplay between twinning and magnesium's macroscopic mechanical behavior [84, 59, 7].

2.3 Modeling Twin Volume Growth

The symmetry of crystalline material microstructure, or the lack thereof, defines the planes on which slip and twinning may occur within said microstructure. Consequently, the texture of a given polycrystalline material, that is the measure uniformity of the crystal orientation of each grain in the material, plays an important role in its mechanical behavior. In simulating this behavior it is critical to accurately account for the evolution of a material's texture during deformation. In calculating the stress and strain fields at each

deformation step with self consistent methods, the antisymmetric spin of each grain is calculated. This represents the rotation of each grain brought on as a result of continued deformation. However, this alone is not sufficient for predicting changes in texture within a polycrystal.

Mechanical twinning as a mechanism for accommodating strain that is otherwise unable to be accommodated by slip represents a significant driving force in the evolution of texture during deformation. As such, any successful simulation of mechanical behavior in materials that experience this phenomenon is predicated on its ability to accurately model the quantity and type of twins expressed therein.

The pioneering efforts of [49] utilized a statistically based criteria for the selection of whole grain orientations for reorientation during deformation. While useful in predicting resulting textures, the empirical nature of this method was incapable of shedding light on the connections between deformation and twin phenomena. Additionally, as whole grains are reoriented to match that of the statistically selected twin system, only the effects of one twin system per grain can be simulated. The later works of [64] explored this link by coupling the growth of twin volume fraction for each twin system with its corresponding strain. In this method, the twin system which first accumulates a predetermined value of twin volume fraction is designated the "Predominate Twin System" (PTS) and the whole grain orientation is rotated to match the orientation of this twin system. In doing this, the PTR inherits one of the limitations of the Van Houte method in which only the effects of the PTS are shown in the resulting texture data.

The Volume Fraction Transfer (VFT) method was able to include the effects of multiple twin systems on texture by the use of a weighted orientation space. In this method, this space is partitioned into orientation subdomains whose volume is proportional to the volume fraction of their corresponding twin system. Deformation by slip is represented in this space by translation vectors applied to the partitions. In this case, the resulting intersection of overlapping sub-domains represents textural changes brought on by deformation by slip. Deformation by twinning is handled in a more straightforward manner where change in twin volume fraction for each system calculated as a function of strain is simply transferred to the appropriate twin orientation partition. While this method was successful in tracking the textural evolution that resulted from multiple active twin systems, it was considered too computationally expensive to be used in polycrystal simulations. As the computational power available to researchers has grown, the VFT method has become progressively more viable.

Similar approaches have been developed that utilize the concept of volume fraction transfer between pre-existing orientations. The works of [57, 35], both utilized a volume fraction transfer approach, albeit with distinct constitutive equations to describe the changes in volume fraction with each deformation step. These methods were applied successfully to the simulation of both FCC and HCP polycrystals. In particular, the work of Gu, Toth, and Hoffman calculated the incremental transfer of volume,ΔV^s, by:

$$\Delta V^s = V_{mother} \times \frac{\dot{\gamma}^s_{twin}}{\dot{\gamma}_{all}} \times \frac{\dot{\gamma}^s_{twin}\Delta t}{\gamma_{twin}}. \tag{2.41}$$

Here, V_{mother} is the weighted volume of the parent or 'mother' grain being reoriented by twinning, γ_{twin} is the characteristic shear of twin system s, $\dot{\gamma}^s_{twin}$ is the shear rate of deformation for the current deformation step of twin system s, and γ_{all} is calculated as

$$\gamma_{all} = \sum_{s=1}^{n} |\dot{\gamma}^s|. \tag{2.42}$$

A similar approach was also adopted in the Twinning De-Twinning model (TDT) developed by [106] in an effort to capture the back and forth transfer of twin volume fraction that occurs under cyclic loading patterns. The TDT model differed from previous works primarily in that separate constitutive equations were used to describe different types of boundary migration, amounting to four effective constitutive laws used to compute twin volume fraction in various states of twin growth or recesion. While this method was capable of generating good simulation results, there is a current disagreement as to the admissibility of the constitutive equations for changes in twin volume fraction in addition to significant computational costs.

2.4 Constitutive Approaches to Hardening Evolution

Nearly every mechanical model for polycrystalline materials simulates the effects of hardening, at least in part, by modifying the critical slip value, τ_c, in the single crystal slip law in Eq. 2.9. In many cases, this power law is adapted to describe shear by twinning, and in this way, the saturation of twinning with increased shear can be simulated. A number of approaches for modeling hardening have been adapted for use in tandem with visco-plastic self consistent methods.

The Voce hardening law is an empirically based model for the evolution of critical resolved shear stress (CRSS) with accumulated strain. Initially developed for slip, the Voce model was later extended to include the hardening of twinning systems as well. Although still widely used, the empirically based curve fitting approach of the Voce model limits its range of application. From this approach, the Mechanical Threshold Stress (MTS) model was developed as an alternative. The MTS model expanded on the Voce model by considering CRSS as a function not only of accumulated shear, but also shear rate and temperature. The work of [19], later developed by [56] and [110], presented an empirical hardening approach which accounted for latent hardening interactions between deformation modes.

The physical motivations behind the hardening of polycrystalline materials have been explored in a number of more recent approaches. The works of [87, 24] both address the role of twin geometry in the impeding of crystallographic slip. In the former, [87] developed a Composite Grain (CG) scheme coupled with the PTR model by which the CRSS is defined as a function of the mean free path between the twin grains of the PTS. In the latter, [24] utilized an Internal State Variable (ISV) approach to track the evolution of the CRSS. This CRSS was defined as a function not only of the mean free path between twin lamella, but also of the angle between the twin plane and the plane of shear for slip. The work of [11] built upon Proust's CG model by adding the consideration dislocation density in the calculation of CRSS. A thermodynamically motivated approach is taken in the model to calculate the changes in dislocation density for each deformation system. These dislocation densities are then used to calculate the changes in CRSS using a Mecking-Kocks type law coupled with the geometric effects of twin boundaries formulated in the CG model.

Beginning with the rate sensitive Hutchinson law, for each deformation mode, α, the shear rate is calculated as

$$d\gamma^{\alpha} = \sum_{s \in \alpha} \dot{\gamma^{s}} dt, \tag{2.43}$$

where

$$\dot{\gamma^{s}} = \dot{\gamma_0} | \frac{m^s : \sigma}{\tau^s} |^n sgn\left(m^s : \sigma\right) \tag{2.44}$$

The critical resolved shear stress and twin propogation terms, τ^s are additively decomposed into hardening contributions from different lower length scale phenomena as

$$\tau_c^s = \tau_0^s + \tau_{forest}^s + \tau_{deb} + \tau_{HP}^s \tag{2.45a}$$

$$\tau_c^t = \tau_0^t + \tau_{HP}^t + \tau_{slip}^t \tag{2.45b}$$

Here the superscripts s and t are used to denote the current slip or twin mode, respectively.

The initial values, τ_0^s and τ_0^t, are Arrhenius type equations capturing the hardening temperature dependence. The terms τ_{forest}^s, τ_{deb}, and τ_{HP}^s represent the contributions to slip hardening from dislocation forests, debris dislocation barriers, and Hall-Petch grain boundaries. These are calculated as

$$\tau_{forest}^s = b^s \chi \mu \sqrt{\rho^s}, \tag{2.46}$$

$$\tau_{deb} = k_{deb} \mu b^s \sqrt{\rho_{deb}} log\left(\frac{1}{b^s \sqrt{\rho_{deb}}}\right), \tag{2.47}$$

and

$$\tau_{\mathrm{HP}}^s = \mu \mathrm{HP} \sqrt{\frac{b^s}{d_g}}. \tag{2.48}$$

Above, τ^s_{forest} is a function of the root of the current system's dislocation density, μ is the shear modulus for the current system. The interaction coefficient, χ is rate and temperature dependent, and typically $0.1 < \chi = \chi s\left(\dot{\epsilon}, T\right) < 1.0$, though it may go as high as 2. In τ^s_{HP}, HP^s is the dimensionless Hall-Petch coefficient and d_{mfp} is the mean free path for the current slip system.

For twinning, the associated contributions are calculated as

$$\tau^t_{\text{HP}} = \frac{HP^{tt'}}{\sqrt{d^s_{mfp}}}, \tag{2.49}$$

and

$$\tau^t_{slip} = \mu \sum_s C^{ts} b^t b^s \rho^s. \tag{2.50}$$

In addition to Hall-Petch and mean free path terms contributing to twin resistence, twin propagation resistence stemming from interactions with slip dislocations is modelled as being proportional to slip system dislocaiton density. Here the Burgers vectors of slip and twin are indicated by the indices α and β respectively. The elements of $C^{\alpha\beta}$ may be greater than or less than 0 depending on whether or not a given slip system impedes or encourages the growth of twin boundary propagation.

The model of Beyerlein and Tomé was successfully applied to the simulation of hardening in Zinc. Built, as it is, on the CG framework, this approach provides a means by which multiple length scales may be bridged in simulation. When implemented in VPSC, contributions from parent and twin grain size and geometry are considered along side the movement and interaction of dislocations in order to provide a comprehensive look into the mechanisms that drive hardening in HCP materials. However, recent studies have illumi-

nated a need for methods that capture not just these two phenomena, but also the manner in which they interact.

CHAPTER III

TASK 1: MODELING THE EFFECT OF PRIMARY AND SECONDARY TWINNING ON TEXTURE EVOLUTION DURING SEVERE PLASTIC DEFORMATION OF A TWINNING-INDUCED PLASTICITY STEEL

Abstract: Modeling the effect of deformation twinning and the ensuing twin-twin and slip-twin induced hardening is a long-standing problem in computational mechanical metallurgy of materials that deform by both slip and twinning. In this chapter, this effect is addressed using the twin volume transfer (TVT) method, which obviates the need of any criterion for twin variant selection. This method is capable of simultaneously capturing at the both primary and secondary, or double, twinning. This is particularly important for modeling in large strain regimes. The modeling methodology is validated by simulating the behavior of an Fe-23Mn-1.5Al-0.3C twinning-induced plasticity (TWIP) steel under large strain conditions experimentally achieved by one and two passes of Equal-Channel Angular Pressing (ECAP) in a 90°die following route BC at 300 °C. Each possible twin variant, whether nucleating inside the parent grain or inside a potential primary twin variant was predefined in the initial list of orientations as possible grains in the polycrystal with zero initial volume fraction. The novelty of the presented approach is to take into account the loss of coherency of the twins with

their parent matrix under large strains, progressively obstructing their further growth. This effect has been captured by attenuating growth rates of twins as a function of their rotation away from their perfect twin orientation, dubbed here as disorientation with respect to the mother grains lattice. This method is implemented in both an isotropic, visco-plastic self consistent code developed at LEM3 as well as the VPSC-7 code from Los Alamos in order to control for difference arising from potential anisotropy. The simulated textures and the hardening under tensile strain showed very good agreement with experimental characterization and mechanical testing results. Furthermore, upper-bound Taylor deformation was found to be applicable for the TWIP steel deformation when all the above ingredients of twinning were captured, indicating that self-consistent schemes can be bypassed.

3.1 Introduction

High-manganese twinning-induced plasticity (TWIP) steels are promising candidates for application in crash-relevant automobile components due to their outstanding mechanical properties [33, 34]. These properties, i.e. high strength, ductility, and work-hardening capacity, originate from their low stacking fault energy (SFE), which is typically in the range between 20 mJ/m2 to 50 mJ/m2 and enables the activation of deformation-induced twinning in addition to planar dislocation slip, while strongly impeding cross-slip [3]. The high work-hardening rates that are responsible for the excellent deformation behavior are attributed to the combination of strong planarity of dislocation motion and the dynamic

Hall-Petch effect that facilitates drastic reduction of the dislocations mean free paths due to the formation of nano-scale deformation twins [16, 17].

Besides their effect on the mechanical properties, the deformation mechanisms active in high-manganese steels have a strong influence on the texture evolution the material. Thus far, this has been analyzed during cold rolling [104, 18, 70, 92, 40, 41, 91, 109], recrystallization [18, 69, 71, 40, 43], and tensile testing [5, 93, 27, 44]. In contrast to the conventional processing of TWIP steels, the severe plastic deformation of these alloys has only been sparsely investigated even though it was found to have a significant effect on their microstructural evolution and mechanical properties [4, 74, 105, 99, 42]. In particular, the understanding of the correlation between deformation mechanisms and texture evolution is limited. In the recent study by [42], the equal-channel angular pressing (ECAP) method was used to deform an Fe-23Mn-1.5Al-0.3C TWIP steel up to four passes at 300 °C following route BC. Experimental analysis revealed that the microstructure during ECAP was continuously refined, owing to both grain subdivision via deformation twinning and by dislocation-driven grain fragmentation. Due to the increased SFE at 300 °C, the latter mechanism dominated the microstructure evolution. In accordance with the correspondence introduced by Suwas et al. [97, 96], a transition texture is formed that contains texture components characteristic of materials with both high and low SFE. Shear bands, if they occur, they appear parallel to the applied shear in shear deformation [61]. As they were hardly observed during ECAP of TWIP steel [39], they were not considered in the present modeling work.

Previously developed methods for modeling the evolution of twin volume fractions and their effects on texture and mechanical hardening begin with the pioneering work of Van Houtte [50] which utilized a statistically based criteria for the selection of parent grains to be reoriented into twin orientations. Later works by Tomé et al. [31] and Lebensohn and Tomé [64] introduced the Predominant Twin Reorientation (PTR) scheme, in which the mother grain is replaced completely by its most active twinning variant once its activity surpasses a critical value. Implemented as part of the viscoplastic self-consistent code, VPSC-7d, the PTR scheme was further developed in order to explore the relationship between twinning and hardening evolution [64, 35, **?**]. However, both methods were limited in that neither allowed for the direct representation of the effects of multiple twin systems on the evolution of texture in simulated polycrystals. Other methods have been developed in order to address this limitation. The Volume Fraction Transfer (VFT) scheme of Tomé et al. [100] calculated changes in texture by discretizing Euler space into separate orientation cells whose centers are occupied by the orientations of physical grains. As the grains are reoriented either continuously through rotations encountered by slip or discontinuously in the case of twinning, the cells in orientation space associated with these grains are shifted via translation vectors or by specific vector transformations for twinning, respectively, in Euler space. The volume fraction of each grain is then modified in an amount proportional to the overlap of the newly positioned Euler cells. The volume transfer approach of Kalidindi [33] is introducing each twinning variant as a physical grain from the beginning and the grain-weights are modified according to the twin activity: volume fractions are transferred from the mother grain to each of the twin-variant as a function of the pseudo-slip

that a twin contributes to the deformation of the mother grain. This technique was adopted for large deformation simulations in recent works of Toth and co-workers to reveal the effect of nano-twins on texture evolution for rolling of ultra-fine-grained copper [34, 35] and for twinning-detwinning activity in fatigue of Mg AZ31 [36]. Twinning in TWIP steel was modelled by Prakash et al. [37], who created only one twin-variant as a new grain, which was selected by the PTR scheme among the 12 possible ones. The full volume transfer scheme for twinning in TWIP steel is applied for the first time in the present work, and without the use of the PTR scheme.

The aim of the work presented in this chapter is to shed more light on the influence of deformation twinning on the texture evolution of face-centered cubic (fcc) alloys with low stacking fault energy, specifically, the high-manganese steel investigated here. To model the texture evolution during ECAP, two different simulation approaches were implemtented. The first, an extended version of the viscoplastic self-consistent (VPSC) polycrystal code, was developed in Metz and had been used [38, 39]. The second was a modified version of viscoplastic self-consistent code, VPSC-7, developed at Los Alamos [cite VPSC sources]. The robustness of VPSC-7 as demonstrated by its widespread application to simulating a variety of materials and load conditions makes it an ideal candidate for providing benchmarks for performance and predicitive power. Both dislocation slip and twinning were implemented into the simulation codes of both approaches by predefining all possible twin variants. The volume fractions of twins were increased according to the activity of the twin systems, which were considered pseudo-slips in their parent grains, without variant selections. In addition to exploring the predicitive capacity of modeling

twin volume growth without the use of twin varient selection criteria, the approach presented herein is novel in that the relationship between the twin and the mother grain in the growth process of the twins is modeled as a function of deviation of twin grain orientations from their ideal twin orientations, relative to the orientation of their parent grain. This deviation, or disorientation, occurs as a consequence of the different lattice rotations of the twin and the parent matrix during the very large strains that are imposed. Finally, the different hardening characteristics of the twins with respect to the matrix are taken into account by a sophisticated self and latent hardening model. This hardening model is benchmarked against the more ubiquitous Voce hardening model.

This chapter aims to answer the following questions:

1. Can the effects of twin volume growth on textural development be simulated effectively without the use of arbitrary twin variant selection methods?
2. Can the overall growth of twin volume fraction of a polycrystal be accurately simulated using the disorientation driven attenuation approach in the absence of empirically based methods for "hardening" said material against further growth of twin volume fraction?
3. More broadly, what light can be shed on the complex interaction between the growth of multiple twin systems, twin grain orientation, and numerical approaches?

3.2 Methods

3.2.1 Experimental Overview

Experimental data for the calibration, verification and validation of the simulation work for this chapter was performed in [102]. Relevant details from the experimental work are presented in this section. As the designation of TWIP steels encompasses a wide range of potential alloys, the chemical composition of the steel investigated in [102] and subsequently used for the calibration, verification and validation of the simulation is detailed in

Table 3.1. The SFEs at room temperature and at 300 °C were calculated to be 5˜25 mJ/m2 and ˜75 mJ/m2, respectively, using a subregular solution thermodynamic model [89].

Table 3.1: Chemical composition of simulated TWIP alloy.

Element	Fe	Mn	Al	C	Si	N	P
wt.%	bal.	22.46	1.21	0.325	0.041	0.015	0.01

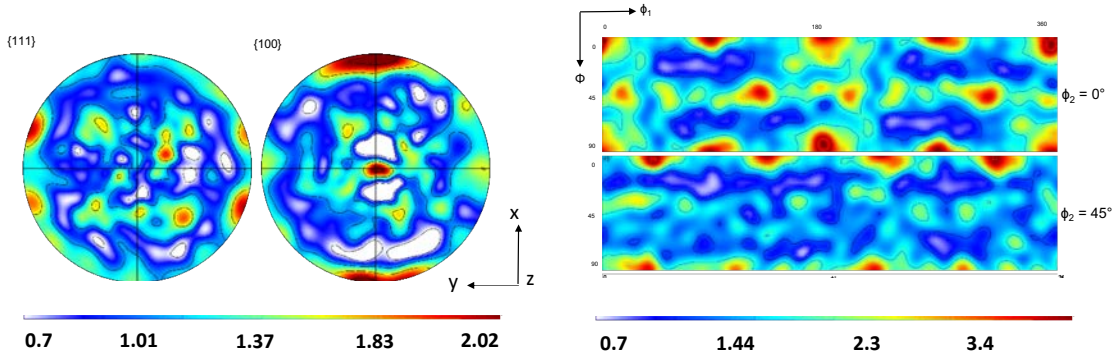

Figure 3.1: Initial rolled texture of TWIP steel.

35 mm rods with a diameter of 10mm sheets were cut from cast TWIP steel subjected to homogenization annealing, forging, and finally hot rolling. These rods were subjected to up to 2 ECAP passes using a 90°die at 300°C following route Bc and a pressing rate of 1mm/s. Specimens for textural analysis were cut from the deformed rods with resulting dimensions of 8mm $\times$ 10mm $\times$ 1mm, along the extrusion, normal, and transverse directions, respectively. X-ray pole figures were generated from three incomplete (0-85°) pole figures along $\{1\,1\,1\}$, $\{2\,0\,0\}$, and $\{2\,2\,0\}$ using a Bruker D8 Advance diffractometer with

an HI-STAR detector, operating at 30 kV and 25 mA using filtered iron radiation and poly-capillary focusing optics. These observations were used to calculate the experimental ODF using JTEX software.

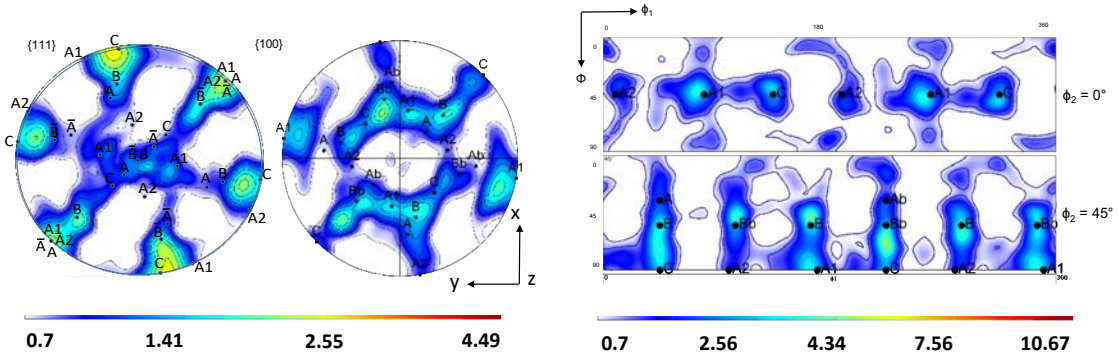

Figure 3.2: Experimental texture after one ECAP pass.

Shown in Figure 3.1, the TWIP steel specimens exhibited a weak texture prior to deformation by ECAP, with the stongest components being the $\{0\,1\,1\}\langle 1\,0\,0\rangle$ cube texture component, with a measured intensity of 2.0 viewed in the $\{1\,0\,0\}$ pole figure. Following the first ECAP pass, shear texture was apparent with stronger A1, C, and B/Bb components and relatively weak A2 and A/Ab. Shear texture patterns continued to be reinforced after the second ECAP pass, with generally higher texture peaks and an ODF maximum between C and B components. These results can be seen in Figure 3.2.

TEM and EBSD measurements of sample specimens revealed not only a significant incidence of twinning, but also that these twins had deviated from their ideal orientations in deformation proceeding their nucleation. Stacks of twin grain lamella with a thickness ranging from 40-100nm were observed. Their angles of deviation, or disorientation, from

the ideal 60°⟨1 1 1⟩ twin orientation was measured to lay within a range of 10°-50°. EBSD images of measured twins and a summary of the angles of disorientation are shown in Figure 3.3 and Table 3.2. Although is has been observed that the twin lamella of TWIP steels preferentially nucleate away from grain boundaries (look up citation) and are, therefore, likely to be completely contained within their respective parent volumes, such measured angles of disorientation suggest that they do not corotate with their parent grains.

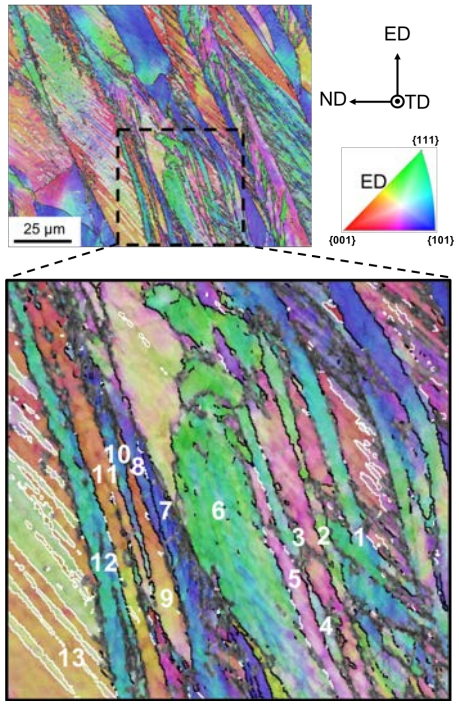

Figure 3.3: EBSD map with color-coding according to the inverse pole figure after one ECAP pass. 13 grains were analyzed. Black and white lines denote high-angle grain boundaries (θ15°) and Σ3 (60°⟨1 1 1⟩) grain boundaries, respectively.

Table 3.2: Orientation relationships between labeled grains in EBSD image.

Combination	Disorientation and nearest rotation axis	Offset from nearest rotation axis (°)	Deviation from twinning position (°)
1-2	$19.07°\langle 3\,\bar{2}\,0\rangle$	6.21	50
2-3	$53.13°\langle 3\,\bar{2}\,0\rangle$	2.47	42.45
3-4	$55.07°\langle 3\,\bar{2}\,0\rangle$	2.57	35.54
4-5	$56.77°\langle 3\,\bar{2}\,0\rangle$	2.39	10.8
5-6	$48.29°\langle 3\,\bar{2}\,0\rangle$	1.87	15.6
6-7	$50.7°\langle 3\,\bar{2}\,0\rangle$	0.47	22.5
7-8	$55.98°\langle 3\,\bar{2}\,0\rangle$	1.98	18.3
8-9	$48.2907°\langle 3\,\bar{2}\,0\rangle$	3.42	8.87
9-10	$58.03°\langle 3\,\bar{2}\,0\rangle$	3.87	10.72
10-11	$58.12°\langle 3\,\bar{2}\,0\rangle$	4.14	28.14
11-12	$55.84°\langle 3\,\bar{2}\,0\rangle$	1.76	9.94
12-13	$56.81°\langle 3\,\bar{2}\,0\rangle$	2.52	9.7

3.2.2 Twin Volume Transfer Constitutive Model

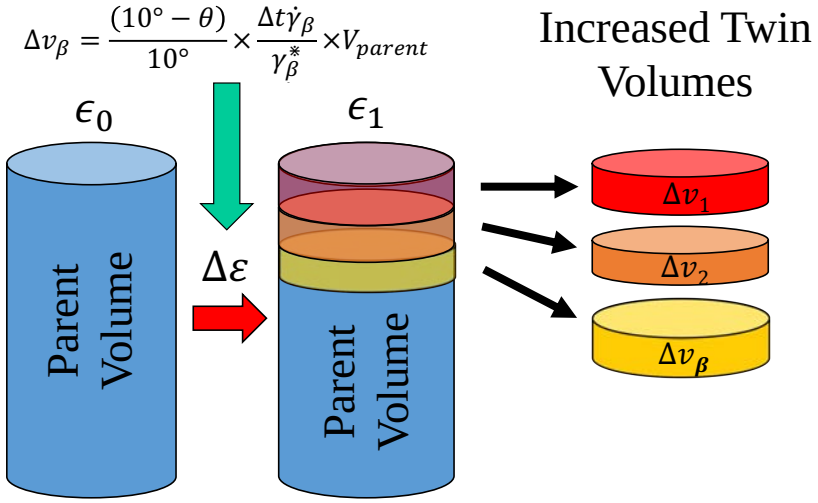

Figure 3.4: Conceptual overview of the twin volume transfer scheme at each deformation step.

Experimental work in [102] observed the evolution of mechanical twin volume fraction in TWIP steels was constrained by the angle of disorientation between between the ideal orientation of each twin system and its actual Orientation relative to the parent grain. While some deviation from ideal twin orientations could still be present during the nucleation of new twin lamella for a given twin system, nucleation was observed to attenuate with significatn growth of this disorientation angle. Shown in Figure 3.4 the twin volume transfer scheme, each potentially activated twin system is represented in a polycrystal simulation by a separate grain orientation with an initial volume fraction of zero. At each deformation step, portions of each mother grain's volume fraction were transfered to volume fractions of grain orientations correpsonding to each of their twin systems. The portion of volume

fraction transfered to each twin system grain, β, was defined as a function of shear on the twin system and the angle of disorientation.

$$\Delta v_\beta = \begin{cases} \dfrac{(10^\circ - \theta)}{10^\circ} \times \dfrac{\Delta t \times \dot{\gamma_\beta}}{\gamma_\beta^\star} \times V_{parent}, & \theta \leq 10^\circ \\ -0, & \theta > 10^\circ \end{cases} . \tag{3.1}$$

Here, θ is the disorientation angle, γ_β is the shear of the the twin system at the current deformation step, and $\gamma_\beta^\star$ is the amount of shear necessary for the nucleation of twin. Here this value is calculated to be $\gamma_\beta^\star = 1/\sqrt{2}$ for the $\langle 1\,,\,1\,,\,2\rangle$ twin system. In this way, twin volume growth is attenuated as the disorientation angle approaches 10°.

In this model, twin grain orientations that had yet to nucleate were tracked, and were subjected to an enforced corotation with parent grains, as the rigid body rotation of a parent grain was applied to each of its corresponding unborn twin grains. Upon nucleation, this enforced corotation was ceased and newly born twin grains were allowed to rotate as separate grains according to it's local stress and strain state. This model was also applied the formation of secondary twins where appropriate.

3.2.3 Models for Hardening Evolution

In order to capture the hardening behavior of the material, two approaches were explored. The first approach was the Bronkhorst type hardening model employed in Kalidindi [57] and Zhou [58]; the second was the Voce hardening model. The Bronkhorst type model defines the critical resolved shear stress, τ_0^α, for a given slip system, α as

$$\dot{\tau}_0^\alpha = \sum_\beta H^{\alpha\beta} |\dot{\gamma}^\alpha|, \quad \forall \alpha, \beta \in 1...n_{slip} \tag{3.2}$$

The generalized hardening matrix $H^{\alpha\beta}$ in Equation 3.2 is calcuated from a slip system interaction matrix $q^{\alpha\beta}$ as

$$H^{\alpha\beta} = q^{\alpha\beta} h_0 \{1 - (\tau_0^\alpha / \tau_{sat})\} \tag{3.3}$$

In Equation 3.3, τ_0^α and τ_{sat} are the actual slip strength and saturation slip strength, respectively, while h_0 is a hardening rate control parameter. The interaction matrix $q^{\alpha\beta}$ is constructed from four distinct values, q_n, corresponding to four potential classifications of slip-slip interactions. q_1, q_2, q_3, and q_4 represent the contributions to hardening of each grain from the interactions between colinear, coplanar, perpendicular, and all other kinds of relative slip-slip orientations, for two slip systems, α and β.

VPSC-7 uses the extended Voce hardening model in which the CRSS of a considered deformation mode is calculated empirically as a function of total accumulated shear in each grain at each deformation step as

$$\tau_{CRSS}^s = \tau_0^s + (\tau_1^s + \theta_1^s \Gamma) \left(1 - exp \left(-\Gamma | \frac{\theta_0^s}{\tau_1^s} | \right) \right). \tag{3.4}$$

In Equation 3.4, τ_0^s is the initial yield value, θ_0^s is the initial hardening rate, τ_1^s is the back-extrapolated yield value, and θ_1^s is the asymptotic rate of hardening.

3.2.4 Implementation

For the simulations utilizing the VPSC polycrystal code developed in Metz, the version fine tuned for finite element implementation was used [38, 39]. The code itself is considered an "isotropic" code, so-called because the interaction between a given grain and the homogeneous medium is calculated using the assumption that the medium itself is

isotropic. Although not appropriate for hexagonal materials, this assumption can be considered valid for cubic materials without strong textures. As TWIP steels possess an fcc crystal structure and usually show weak textures [46], such conditions were assumed to be met. The volume transfer scheme recently introduced in publications by Toth et al. to account for twinning [35, 36] was implemented in the VPSC code; simultaneously for both primary and secondary twinning.

The Los Alamos code, VPSC-7d, was modified, replacing the the PTR scheme implemented in SUBROUTINE UPDATE_TWINNING with the TVT scheme implemented in SUBROUTINE UPDATE_TWINNING_VTT. Unlike the Metz code, VPSC-7 is an "anisotropic" code, in that the homogeneous polycrystal medium is not assumed to be isotropic, thereby extending its domain of application to polycrystal materials with low crystal symmetries. As with the Metz code, simulations were carried out with both primary and secondary twinning actively considered during the simulation.

3.2.5 Simulation

The simulation work of this chapter was performed along two parallel research "channels". In the first, the TVT model without disorientation driven attentuation was used to simulate a single ECAP pass in order to provide a control for ongoing comparison. SImulations were performed using both Taylor approximations and the self-consistent approaches. The disorientation driven attenuation was then added to more accurately capture the texture evolution. In the second, the TVT model was implemented in VPSC-7 and used to simulated the same ECAP pass using the same approaches. The choice to perform

these simulations using both codes was motivated by the desire to see the effects, if any, that assumptions regarding the (an)isotropy of the polycrystal medium would have on the predictive capacity of the TVT approach.

In both cases the simple shear model for ECAP with a 90°die was utilized to define the velocity gradient of the bulk material. The simulation of a single ECAP pass was performed across 40 deformation controlled steps, defined by an equivalent Von Misses strain increment of $\Delta\epsilon_{VM} = 0.028867$, corresponding to a total shear strain of $\gamma = 2.0$ on the 45°plane of shear. This approach is shown in Figure 3.5. In simulations for the first ECAP pass using the Metz self-consistent code, only primary twinnning was activated in the code, as no secondary twinning was observed experimentally under this condition. This led to the consideration of 500 parent grains with 6000 (12 twin variants per parent) potential twin grains for the initial texture. In simulations for the second ECAP pass, this number was increased to include 12 secondary twin grains for each primary twin grain, for a total of 78500 grains. For simulations using VPSC-7, only on ECAP pass was simulated. While secondary twinning was considered potentially active in the sense that the capability of secondary twin volume fraction to occure was turned on, no volume fraction of secondary twins was observed to have accrued in pilot simulations. In light of the experimental observations from the single ECAP pass experiments, secondary twinning was turned on in the primary twin "phase" and tracked as a variable rather than being tracked as an additional "phase" unto itself in the name of minimizing computational costs associated with the final simulations. This resulted in 6500 total grains being tracked with 500 in the parent "phase" and 6000 twins in the other. In the cases of both codes, simulations were carried out us-

ing both a Taylor equivalent assumption and a self-consistent approach using the Tangent modulus.

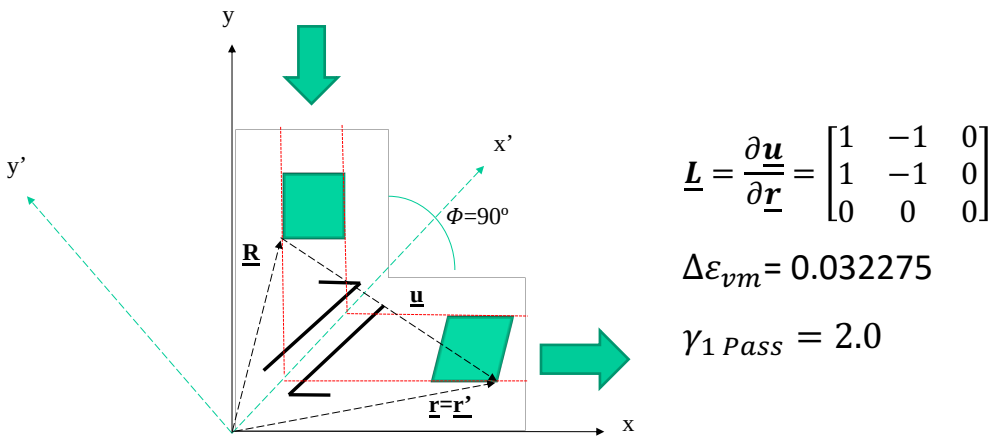

Figure 3.5: Simple shear model for a single ECAP pass.

3.2.6 Calibration

Before beginning ECAP simulations in earnest, hardening coefficients for both the Bronkhorst type model of and the Voce hardening model in VPSC-7 were obtained by fitting simulated stress curves of the TWIP steel in it's initial hot-rolled state to experimental data obtained by subjecting pre-ECAP samples to uniaxial tension producing a twin volume fraction of 0.2 and 0.28, respectively, at $\epsilon = 0.4$. A comparisson of the fitted tensile curves is presented in Figure 3.6 along with the corresponding hardening and modeling paramters f or the Bronkhorst type model in Table 3.3.

Table 3.3: Modeling parameters for Metz VPSC simulations.

Slip mode and initial strength, τ_0	$\{1\,1\,1\}\langle 1\,1\,0\rangle$, 167 MPa
Twinning mode and initial strength, τ_0	$\{1\,1\,1\}\langle 1\,1\,2\rangle$, 167 MPa
Hardening rate for parent grain, h_0	163.5 MPa
Hardening rate for primary twin, h_0	327 MPa
Hardening rate for secondary twin, h_0	489 MPa
Saturation Stress, τ_{sat}	1650 MPa
Strain hardening parameter, a	0.5
Latent hardening parameters	$q_1 = 1$, $q_2 = 1.2$, $q_3 = 2$, $q_4 = 1.5$
Strain rate sensitivity parameter for slip and twinning, m	0.166
Interaction coefficient for Tanget VPSC model, α	0.166
Total number of grains for primary twinning	6500
Initial grain shape aspect ratios for twin grains	1:5:5

An iterative process was used for the fitting for τ_0 for both slip and twinning, τ_{sat}, α, and h_0 for parent, primary twin, and secondary twins. The definitions of q_n led to the constraints $q_1 < q_2 < q_3$ on their fitted values. The value of q_4 was not constrained by any specific physical process, and so was taken as the average value of q_1, q_2, and q_3.

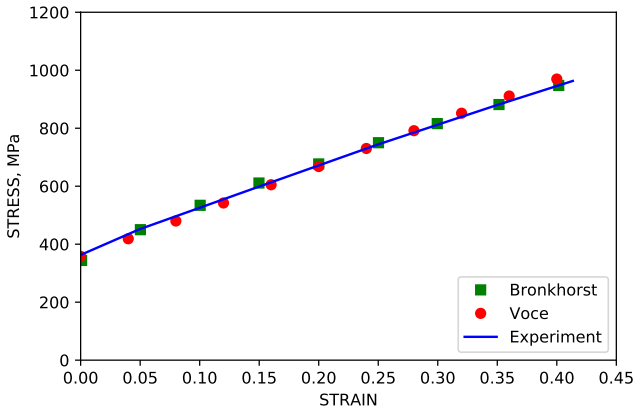

Figure 3.6: Fitting curves for TWIP steel subjected to uniaxial tension.

For simulations using VPSC-7, the total volume fraction of primary twins was considered to be a separate "phase". In this way, the incidence and growth of both primary and secondary twins could be tracked in the event that they should occur. As cross slip and Hall-Petch effects are not explicitely considered in the Voce model between different grains except through the empircal effects of latent hardening parameters, the consideration of twin volumes as separate phases within the implementation yielded an opportunity to try and capture the effects of twin volume growth on overall polycrystal hardening by assigning them a set of Voce hardening parameters that differed substantially from those of the parent phase. The observed rigidity of twin lamella was approximated with initial

CRSS for slip τ_0 for slip systems in the twin "phase" of twice that of slip systems in the parent grain. The hardening parameters for the Voce hardening model from the tensile fitting are summarized in Tables 3.4 and 3.5

3.3 Results

3.3.1 1^{st} ECAP Pass

The results of the simulations of a single ECAP pass performed using the Metz self-consistent code showed marked differences between the Taylor equivalent and self-consistent approaches. Shown in Figure 3.7, peaks in the Euler sections viewed at $\phi_2 = 0°$and $\phi_2 = 45°$associated with the A1, C, and B/Bb texture components expressed in the experimental data are clearly visible. Viewed along the $\langle 1\,1\,1 \rangle$ and$\langle 1\,0\,0 \rangle$ directions, the simulated pole figures shown in Figure 3.7 exhibited clear sheared textures associated with strain conditions of ECAP. Although the intensity of these peaks was noticeably higher than the intensity of the peaks in the experimental measurements, such discrepancies are common in simulation work. Shown in Figures 3.8, self-consistent methods performed with the Metz code both underpredicted the A1, B, and C texture components, while overestimating the incidence of A and A2 components.

Table 3.4: Parent grain hardening parameters for VPSC-7 simulations.

$\{1\,1\,1\}\langle 1\,1\,0\rangle$ Slip mode: Parent Grain	
Initial yield strength, τ_0	250 MPa
Back extrapolated yield strength, τ_1	0 MPa
Initial hardening rate, θ_0	350 MPa
Asymptotic hardening rate, θ_1	350 MPa
$\{1\,1\,1\}\langle 1\,1\,2\rangle$ Twin mode: Primary Twin	
Initial yield strength, τ_0	250 MPa
Back extrapolated yield strength, τ_1	0.0 MPa
Initial hardening rate, θ_0	150 MPa
Asymptotic hardening rate, θ_1	150 MPa
Initial grain shape aspect ratios for twin grains	1:1:1

Table 3.5: Twin grain hardening parameters for VPSC-7 simulations.

$\{1\,1\,1\}\langle 1\,1\,0\rangle$ Slip mode: Twin Grain	
Initial yield strength, τ_0	560 MPa
Back extrapolated yield strength, τ_1	0 MPa
Initial hardening rate, θ_0	400 MPa
Asymptotic hardening rate, θ_1	400 MPa
$\{1\,1\,1\}\langle 1\,1\,2\rangle$ Twin mode: Secondary Twin	
Initial yield strength, τ_0	800 MPa
Back extrapolated yield strength, τ_1	0.0 MPa
Initial hardening rate, θ_0	300 MPa
Asymptotic hardening rate, θ_1	300 MPa
Initial grain shape aspect ratios for twin grains	1:5:5

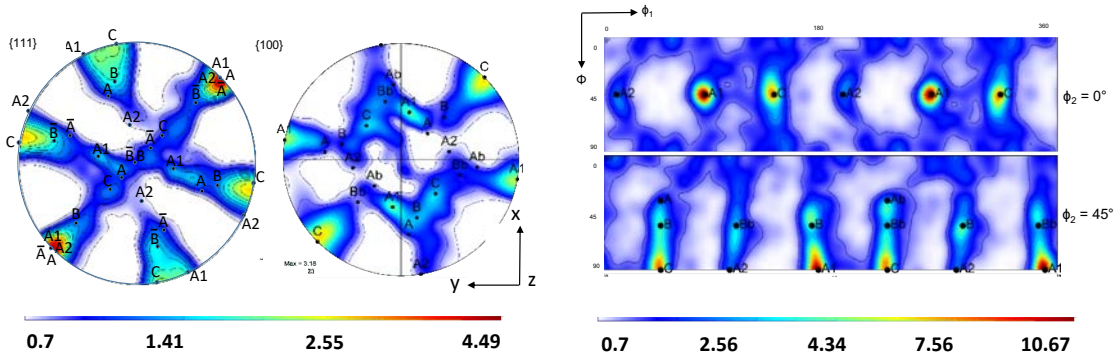

Figure 3.7: Texture simulations of one ECAP pass using the Taylor approach in the Metz self consistent code.

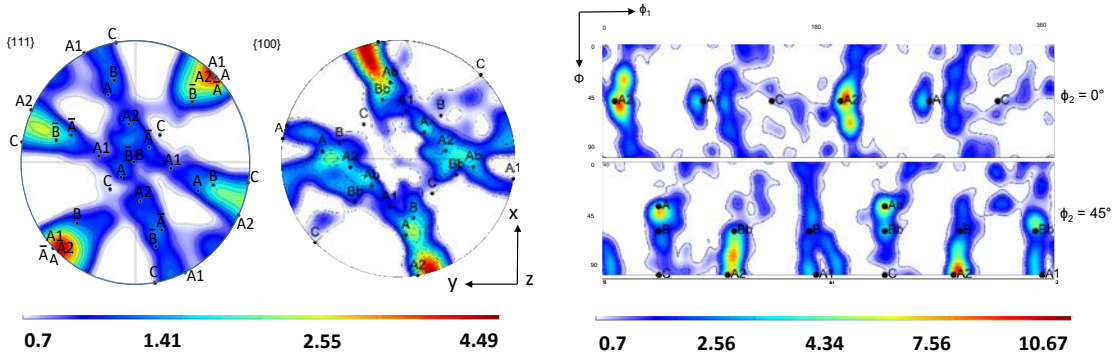

Figure 3.8: Texture simulations of one ECAP pass using the tangent, self consistent approach in the Metz self consistent code.

Simulations performed using VPSC-7 yielded similar results to the Metz code. Peaks in the $\phi_2 = 0°$and $\phi_2 = 45°$Euler sections performed with the Taylor equivalent constraints were consistent with the texture components of both the experimental texture readings and the Taylor simulations produced using the Metz self-consistent code. Self-consistent

simulations using the Tangent modulus also overestimated A and A2 components while simulatneously producing skewed B type texture components. These results are shown in Figures 3.9 and 3.10 for Taylor and self-consistent approximations, respectively.

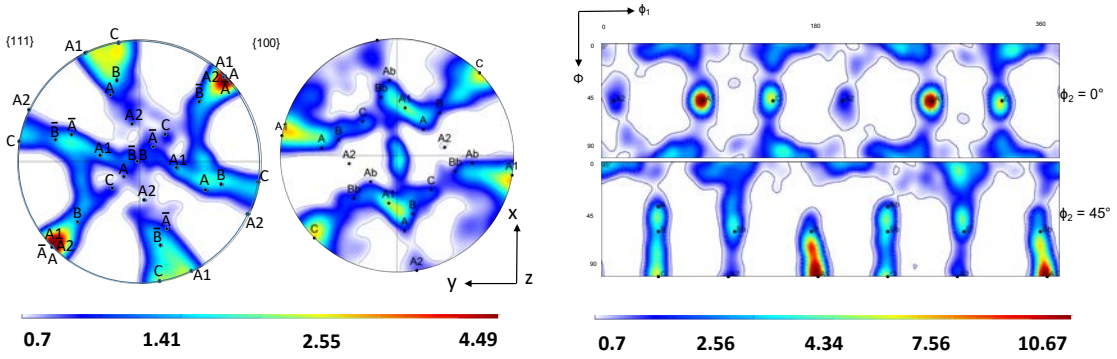

Figure 3.9: Texture simulations of one ECAP pass using the Taylor approach in VPSC-7.

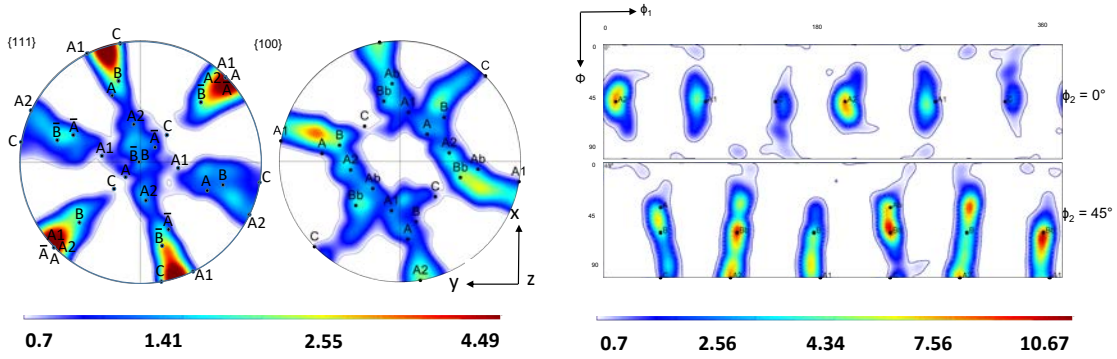

Figure 3.10: Texture simulations of one ECAP pass using the tangent, self consistent approach in VPSC-7.

Simulated twin volume fraction reached 48% and 40% at the end of the ECAP pass for the Metz code and VPSC-7, respectively as shown in Figure 3.11. In Figure 3.12, the

average angle of disorientation of nucleated twin grains from their ideal twinning angles for their corresponding twin variant is seen to be monotonically increasing with equivalent strain, to an average of approximately 13°at the end of the single ECAP pass. Figure 3.13 reveales that twin disorientation spanned a range from 0°to 50°, with twin disorientation skewing towards only small deviation from ideal twinning positions at the end of single ECAP pass, as well.

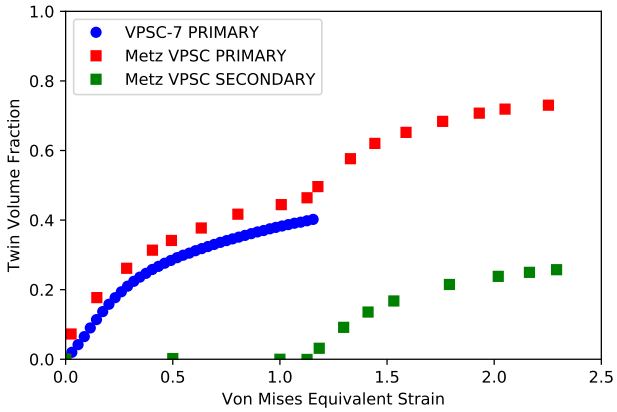

Figure 3.11: Twin volume evolution for ECAP.

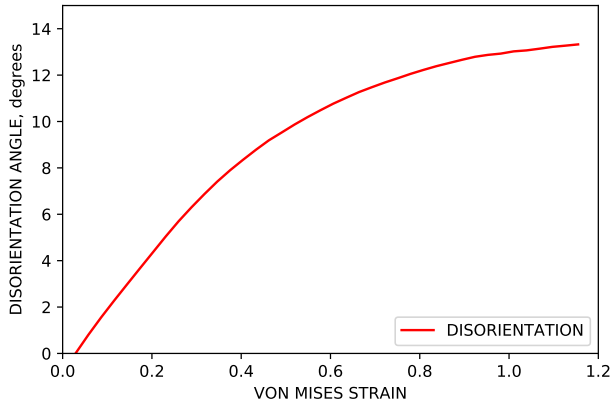

Figure 3.12: Evolution of average disorientation angle during one ECAP pass.

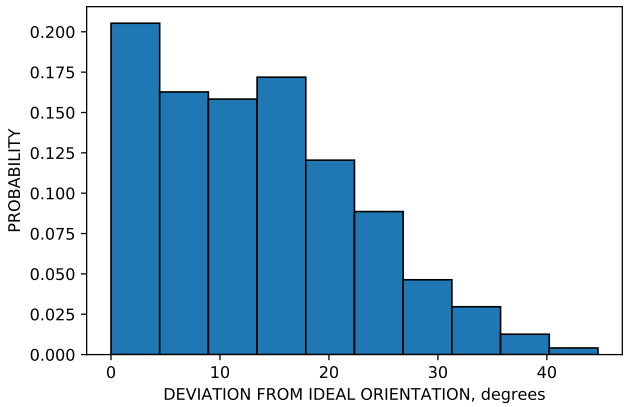

Figure 3.13: Probability distribution of final twin grain deviations from ideal positions.

3.4 Anaylsis

In summary, simulation trends reveal a few key points that must be addressed:

1. Simulated twin volume fraction was, in general, higher than past values observed experimentally [38, 42].
2. Simulated textures yielded good agreement with experimental results when simulations were performed using the Taylor approach. Self-Consistent approaches using the tangent modulus in both codes were less accurate with respect to the experiment, with A2 and A texture components being overestimated, with A1, B, and C components being underestimated in both the Metz and modified Los Alamos code. Additionally, in all cases, simulated textures showed sharper peaks at concentrations of texture than those observed in experiments.

When considering item number one, above, it must be noted that current techniques for EBSD imaging suffer from two notable limitations which may lead to the underestimation of twin volume fraction when applied to TWIP steels. First, EBSD measurements of twin volumes become significantly more difficult in the case of materials whose twin grains exhibit a thickness and intergranulare spacing on the scale of nanometers. The particular geometry of twin lamella inside TWIP steels, then, represents a twinning texture for which EBSD techniques may struggle to identify the totality of twin volume fraction. Furthermore, EBSD is unable to capture twin grains that have migrated from their ideal twinning orientations. As shown in the experimental observations summarized in Table 3.2 and reinforced by simulation results shown in Figure 3.13, substantial deviations from such positions were observed. As such, this represents a signficant source of potential error, skewing results towards underestimation of twin volume fraction in EBSD measurements for TWIP steels subjected to ECAP. Taking both of these limitations into consideration, such relatively high simulated twin volume fractions are much more reasonable [38].

Item number two requires more comprehensive discussion. The more pronounce peaks in simulated texture observed in all cases can be contextualized when viewed in conjunction with their numerical contribution to fraction of texture components in the ODF. Figure **??** shows the volume fractions of orientations as they contribute to texture components in the simulated ODFs. Peak values of these contributions do not exceed even a single percent in both Taylor and SC approaches, placing the error of estimation for each simulation within the range of a fraction of a percent. Consequently, simulated textures presented herein fall within an acceptable bound of numerical error.

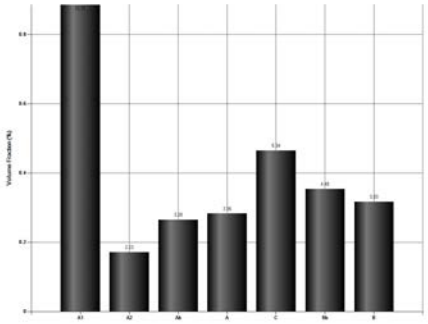

Figure 3.14: Contributions to texture components in simulated ODFs for Taylor simulations.

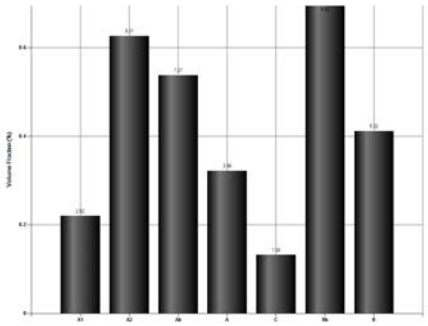

Figure 3.15: Contributions to texture components in simulated ODFs for self consistent simulations using the tangent modulus.

As shown in the work of [102], the simulated texture of TWIP steel under ECAP more successfully modeled under the fully constrained Taylor approach, thereby bypassing additional computational costs associated with more complicated sef-consistent methods. Under the Taylor approach for polycrystal modeling (not to be confused with the Taylor approach for slip in single crystals), homogeniety of deformation throughout a polycrytal is enforced by assuming that velocity gradients at the crysal level are indentical to those experienced by the polycrystal sample. While computationally expedient, such conditions are not always observed in polycrystals. The relative accuracy of the Taylor approach when compared to self-consistent methods as implemented in the Metz code and confirmed in VPSC-7 suggest that some form of enforced compatibility exists within a given grain. Such a confirmation also supports the idea that the homogeniety of strain is agnostic with respect to the the hardening approach, and therefore a consequence of the polycrystal modeling approach and not the specific constitutive relationships, implying real material conditions that closely mirror the kinematic assumptions. This is further supported by the fact that differ-

ences in simulated textures between the isotropic Metz code and the anisotropic VPSC-7 were most pronounced in SC approaches. While key features such as the overabundance of A2 texture components and the under representation of A1 and C components were seen in both codes, the simulated texture of the isotropic codes was noticeably more disperse.

As posited in [102], this may be explained when the high simulated twin volume fraction addressed in point one is taken into consideration. TWIP steel is nucleation controlled, that is, twin volume growth is achieved not by the migration of twin boundaries and expansion of exsiting twin grains, but by the nucleation of new grains. The twins themselves are generally accepted to be much harder than untwinned regions [24, 2, 37, 38]. Additionally, the spacing between twin grains with stacks of twin lamella is relatively small, on the order of 30-50 nm as stated earlier. These characteristics of twinning in TWIP steel combined with the higher than expected twin volume fraction supports the supposition that twin grains may act as a kind of "skeleton" or frame, embedded within the untwinned regions. The relative rigidity of this frame could serve to motivate enforced compatibility of strain within a grain which had accumulated sufficient twin volume fraction, especially in a localized region around grain boundaries. Observed dislocation pileup and the absence of void nucleation in the intergranular region between twin grains is consistent with this theory [38].

In order to verify that the simulated textures presented in this work are the result in part due to the successful application of the TVT model for twin growth, two reference textures were generated. The Euler sections in Figure 3.17 show the twinned orientations of ideal components after ECAP at $\phi_2 = 0°$and $\phi_2 = 45°$. Here concentrations of A1,

B, and Bb components are clearly visible. Pictured in Figure 3.16 are the ideal texture components associated with the shear experienced under 90°ECAP. In this figure, peaks are seen aligned with the positions of the A2, B, and C components , while A1 components are non existent. Taken in conjunction with each other, these two textures suggest that reorientation by twinning in TWIP results in the redistribution of A2 components to the A1 orientation. B and Bb components, which twin into each other's orientations, would remain strong, as would C components. This is consistent with the results of the experiemental textures and Taylor simulations for both the Metz and VPSC-7 implementations. This suggests that the TVT scheme can capture the texture evolution driven by twin growth and attenuation with a reasonable degree of accuracy.

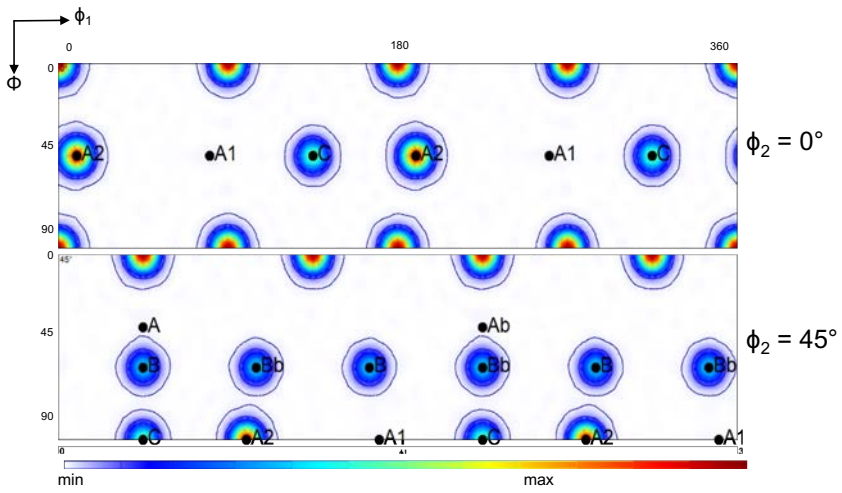

Figure 3.16: Texture associated with shear after a single ECAP pass.

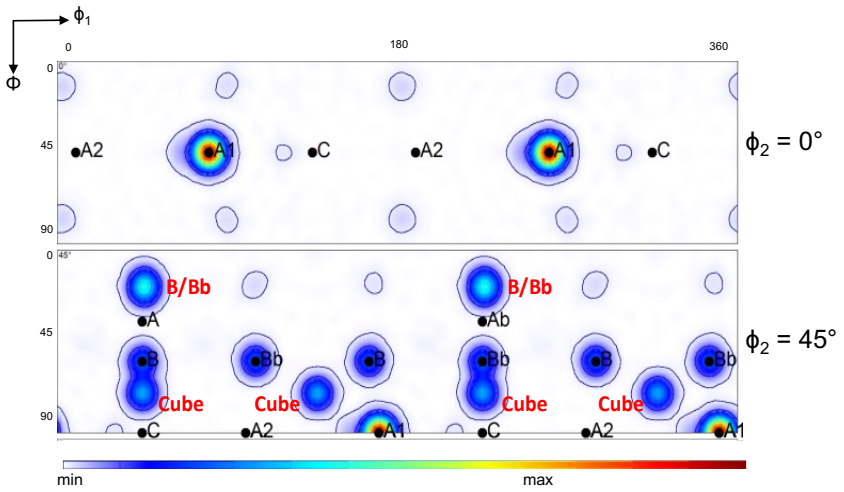

Figure 3.17: Texture associated with ideal twin positions after a single ECAP pass.

3.5 Conclusion

In this chapter, the texture evolution of hot rolled, low SFE, TWIP steel subjected to a 90°ECAP pass following route Bc was simulated using both the Metz self-consisent and Los Alamos VPSC-7 codes, with and without assumed isotropy in the simulated poly-crystal medium. In both codes, simulations were carried out under both fully constrained Taylor assumptions, and self-consistent approaches using the tangent modulus. In all cases, twinning effects were modeled using the TVT scheme which simultaneously considers the effects of multiple twin variants on texture. In the TVT scheme, twin volume growth for each variant is described by a consitutive law that considers the attenuation of growth as a function of the angle of disorientation between th twinned grain and its corresponding ideal twinning position relative to its parent grain. Hardening parameters for a Bronkhorst type hardening approach and the Voce hardening model were obtained by fitting to the material subjected to uniaxial tension for the Metz self-consistent code and VPSC-7, resp-

sectively. Hardening effects due to the onset of twinning were modeled in the Metz code using latent hardening parameters, while the interaction of slip and twin grains in VPSC-7 was approximated by considering twins as a separate, harder, phase.

Simulated texture results using the Taylor approach match well with the experimental data in both codes, with tangent approaches yielding less agreement. Twin volume fraction was generally higher than published EBSD experiments, but this may be attributed to the limitations of the technique to fully approximate the volume fraction of an observed material when twin grains rotate outside of their ideal twinning orientations rather than the failure of the attenuation driven constituive law to accurately model twin growth. In both codes, the disorientation of twin grains from their ideal orientations was reasonably captured.

This leads to the following conclusions for the driving questions presented at the beginning of this chapter.

1. Textural effects of twinning can be captured without the need for arbitrary twin variant selection methods, *a la* PTR method in cases of severe plastic deformation. With increases in available computing power, variant selection based methods may not always be the most favorable approach should methods that give simultaneous consideration to multiple twin variants be shown to have predictive value for a broader range of strain regimes and polycrystal materials.
2. Although the final levels of twin volume fraction were higher than shown in previous experiments, such a difference can be explained by the limitations of current imaging techniques. In this case, simulations using the disorientation driven attenuation implemented in the constitutive law alone were able to recreate twin volume growth curves seen in simulations using latent hardening in high strain regimes.
3. In the particular case of TWIP steels, the Taylor approach to polycrystal simulation was shown to have greater predictive power for the purpose of texture evolution in ECAP than the self-consistent models using the tangent modulus, suggesting that the internal state of the polycrystal is one of enforced compatibility. This may obviate the need for more computationally costly self-consistent models in the case of simulating TWIP steels.

CHAPTER IV

TASK 2: CRYSTAL PLASTICITY MODELING OF ABNORMAL LATENT HARDENING EFFECTS DUE TO TWINNING

Recent characterization studies using transmission electron microscopy as well as advanced molecular dynamic simulations have shown that slip dislocations whether striking or struck by a $\{1\,0\,\bar{1}\,2\}$ twin boundary dissociate into a combination of twinning disconnections, interfacial disclinations (facets), and other types of dislocations engulfed inside the twin domains, called transmuted dislocations. While twinning disconnections were found to promote twin propagation, the dislocations incorporated inside the twin are of considerable importance to hardening and damage initiation as they are doomed to more significantly obstruct slip dislocations accommodating plasticity of the twins. In this paper, the dislocation transmutation event and its effect on hardening is captured using a dislocation density based hardening model implemented in the viscoplastic self consistent code, VPSC-7. This is done by allowing the twins to increase their dislocation densities, not only by virtue of slip, but also through dislocations that transmute from the parents as the twin volume fraction increases. A correspondence matrix rule is used to determine the type of converted dislocations while tracking and parameterizing their evolution. The model acknowledges a new physics-

based mechanism and is expected to canalize current fitting approaches of hardening in hexagonal materials which relied thus far on twin-induced lattice reorientation and Hall-Petch mechanisms.

4.1 Introduction

The utilization of hexagonal-close packed (HCP) magnesium (Mg) and magnesium based alloys is of interest to industry because of their low density and high specific strength. Their low crystal symmetry leads to mechanically anisotropic behavior in highly textured textured condition in which significant nucleation and growth of $\{1\,0\,\overline{1}\,2\}$ tensile twins may occur. The profuse twinning of Mg produces brittle properties in the material that makes it unsuitable for many applications. In order to expand the range of industrial applications of magnesium and its alloys, the contributions of twinning to the mechanical behavior of the material must be better understood. Multiscale simulations serve a dualistic role in modern material investigations by both guiding and being guided by physical experiments. In the case of magnesium and its alloys, crystal plasticity based simulations are useful bridging the gap between lower length scale phenomena and continuum scale material behavior.

Studies of single crystal magnesium revealed that slip along the basal and prismatic planes are often active during deformation, both possessing a relatively low CRSS when compared with other deformation modes [13, 22, 47]. However, in order to accommodate deformation along the c-axis, pyramidal-$\langle c + a \rangle$ slip and tensile $\{1\,0\,\overline{1}\,2\}$ twinning modes can be needed as well, leading to heavily anisotropic behavior, both observed experimentally and predicted in polycrystal modeling [26, 82, 68, 60, 52]. In some cases highly

profuse twinning in which 80% of the parent grain volume is overtaken by twin volume fraction can occur. In other cases scarcely no twinning at all may take place [13, 47, 8, 53]. Consequently, a number of studies have focused on slip-slip, slip-twin, and twin-twin interactions [28, 54]. Because twinning generates new grains within a given parent grain, it is reasonable to assume that the hardening evolution of magnesium is driven by a Hall-Petch (HP) type mechanism as the newly generated twin grain boundaries were thought to impede the motion of dislocation slip within the parent grain, and many modeling approaches were developed which considered this phenomena as a signficant driver of mechanical hardening due to slip-twin intereaction in Mg and its alloys, and therefore, a prime actor in their anisotropic behavior [78, 28, 86, 23].

The work of [83] demonstrated that, rather than being caused by HP effects, this anisotropy could be the result of increased dislocation density inside the twin grains. Implementing a modified version of the dislocation density based hardening model of [11] in the viscoplastic self-consistent (VPSC) code (VPSC-7d from Los Alamos National Laboratory) the compression of rolled Mg with a highly basal texture along multiple compression loading paths were simulated. By setting the contributions of HP mechanisms to zero, [83] showed that increasing the amount of dislocation density stored inside twin volumes by a Twin Storage Factor (TSF) recreated the characteristic hardening behavior across multiple load paths. This approach will be referred to as the TSF method in the following. This demonstrated that the assumptions about how slip dislocations interact with twin grain boundaries may require additional investigation in order to be completely understood. More specifically, it was shown that increasing the dislocation density of twin

grains could reproduce hardening reactions previously thought to have been caused solely by Hall-Petch effects. However, this empirical approach was limited in that the specific physical process by which dislocation density was increased inside of twin grains was not modeled.

The findings of [83] were bolstered by the molecular dynamics (MD) work of [53]. In that work dislocations on the $\{0\,0\,0\,1\}$ basal plane that encountered a $\{1\,0\,\bar{1}\,2\}$ tensile twin grain boundary were shown to either facilitating twin boundary movement by dissociating into twinning disconnections, or transmute into dislocations along different slip systems inside the twin volume fraction depending on the relative geometry of the dislocation and the twin boundary. Though the complete dislocation reaction at the twin interface was only recently identified by means of atomistic simulations and advanced interfacial defect theory, the part of the dissociation leading to dislocation transmutation has been hypothesized as early as the nineteen sixties by Bilby and Saxl and was later known as the Basinski mechanism [14, 94, 9]. Similar to the Basinski mechanism [9], the capacity of dislocations to transmute from parent grains across twin boundaries represents a potential vehicle by which the dislocation density of twin grains might be increased in excess of statistically and geometrically necessary dislocations typically formed to accommodate slip within the twin. Transmutation could then account for the increased dislocation density enforced by the twin storage factor of [83]. While previous studies have conceded that a Basinski type transmutation effect may be occuring in twinning Mg, experimental evidence has been sparse thus far [23, 78, 28]. Although the mechanisms by which Basinski like transmutation may take effect have been studied, there are few treatments in the literature on how

to incorporate these mechanisms in constitutive laws in order to "up-scale" their effects on grain behavior [25]. The work of [55] provides a crystal plasticity framework by which such transmutation effects might be modeled in VPSC simulations. They developeded a transmutation matrix α where each element α_{ij} represents the proportion of dislocation density that is transmuted to the i^{th} slip mode inside the twin volume from the j^{th} slip mode in the parent volume.

The work of this chapter introduces a modified version of the crystal plasticity based dislocation transmutation theory of [55], further adapted to capture the mode-wise nature slip dislocation interaction with twin boundaries and allow for the inclusion of both transmutation and disassociation behavior of these dislocations. In this way, a physically based model for the complex interactions of slip and twinning in polycrystal Mg is developed. This model is implemented the LANL code VPSC-7d, calibrated using assumptions based on the findings of the MD work [53] and the application of the correspondence method of [14], and used to simulate the anisotropic hardening behavior of rolled Mg under multiple compression load paths. This is done with intention of answering the following research questions:

1. To what extent is the hardening behavior of Mg informed by the processes of dislocation transmutation and dissociation across twin grain boundaries?
2. Is hardening by dislocation transmutation alone enough to account for the anisotropic hardening behavior of Mg, or can it be reasonably concluded that this process merely supplements Hall-Petch type effects.
3. To the extent that hardening in Mg is informed by transmutation effects, how does this effect the evolution of dislocation density.
4. Can transmutation be implemented in the absence of arbitrary curve fitting procedures based on empirical findings without sacrificing predictive capacity?

4.2 Methods

4.2.1 Model

The model for this work is based on the approach of [11] in which the hardening behavior of HCP polycrystals is simulated by the evolution of the critical resolved shear stress (CRSS) used in Hutchinson'sstrain rate sensitive constitutive equation. In this approach, the CRSS for slip in each slip system s in the slip mode, i, is defined as a function of the dislocation density on that system. The CRSS of each system was given by the additive decomposition

$$\tau_c^s\left(\rho^i\right) = \tau_0^i + \tau_{forest}^i\left(\rho^i\right) + \tau_{deb}^i\left(\rho^i\right) + \tau_{HP}^s, \quad \forall s \in i. \tag{4.1}$$

Here, τ_0^i, τ_{forest}^i, τ_{deb}^i, and τ_{HP}^s are the initial critical stress value, hardening from forest dislocations, hardening from debris formation, and hardening from Hall-Petch effects, respectively. They can be defined as

$$\tau_{forest}^i\left(\rho^i\right) = b^i \chi \mu \sqrt{\rho^i}, \tag{4.2a}$$

$$\tau_{deb}^i\left(\rho^i\right) = k_{deb}\mu b^i \sqrt{\rho_{deb}} \log\left(\frac{1}{b^i\sqrt{\rho_{deb}}}\right), \text{ and} \tag{4.2b}$$

$$\tau_{HP}^s = \begin{cases} \mu\text{HP}^i \sqrt{\frac{b^i}{d_g}} \text{ for grains without twins,} \\ \mu\text{HP}^{ij} \sqrt{\frac{b^i}{d_{mfp}^{s,PTS}}} \text{for grains with twins.} \end{cases} \tag{4.2c}$$

In Equation 4.2a, b^i and ρ^i are the Burgers vector and dislocation density on the i^{th} slip mode. χ and μ are the dislocation interaction coefficient and shear modulus, respectively. Equation 4.2b also contains the debris formation parameter k_{deb} and debris density ρ_{deb}. The Hall-Petch contributions in Equations 4.2c depend on the presence of twins. In grains

where there is no active twinning, these contributions are the same for all $s \in i$, with a bulk interaction term HP^i and grain size d_g. In the case of grains with a predominate twin system j, the interaction term HP^{ij} describes the interaction between twin mode j and slip mode i. Here, $d_{mfp}^{s,PTS}$ is the mean free path between twin lamella described in [86].

In the simulations presented in this work, the forest and debris contributions remain unchanged. However, the constitutive model of [11] is based on the Composite Grain (CG) model of [86] and treats twin boundaries as full-stop barriers to dislocation glide. As twin boundaries are not considered to act as barriers in this work by hypothesis, the Hall-Petch contributions to CRSS are treated as being identically zero, hence

$$\tau_{HP}^{s} = 0, \quad \forall s \in i. \tag{4.3}$$

In the model of [11], the change in dislocation density for a given slip mode α with change in shear on the same system is calculated by a Mecking-Kocks [75] type equation and adopted in this work to calculate the change in dislocation density with shear as

$$\frac{\partial \rho^i}{\partial \gamma^i} = k_1^i \sqrt{\rho^i} - k_2^i \left(\dot{\epsilon}, T\right) \rho^i. \tag{4.4}$$

Equation 4.4 introduces the phenomenological generation and rate and temperature dependent parameters k_1^i and k_2^i. There is a relationship between these two parameters,

$$\frac{k_2^i \left(\dot{\epsilon}, T\right)}{k_1^i} = \frac{\chi b^i}{g^i} \left(1 - \frac{kT}{D^i (b^i)^3} log\left(\frac{\dot{\epsilon}}{\dot{\epsilon}_0}\right)\right). \tag{4.5}$$

Above, g^i, D^i are the normalized activation energy and drag stress, respectively, and $\dot{\epsilon}$ and $\dot{\epsilon}_0$ are the strain rate and reference strain rate.

In the present model, the dislocation densities were modified based on changes in twin volume fraction of the composite grain, which were added:

$$\rho^{iTF} = \begin{cases} \rho^{i}, & \forall s \in \text{parent volume fraction} \\ \rho^{iTF}\left(V\right), & \forall s \in \text{parent volume fraction.} \end{cases} \tag{4.6}$$

In this way, the hardening contributions from dislocation density to the CRSS of slip systems inside the twin volume fraction of each grain are differentiated from those systems inside the parent volume fraction.

The function $\rho^{iTF}\left(V\right)$ from the work of [55] defining the increase in dislocation density of the i^{th} slip mode type inside the j^{th} twin volume fraction is expressed as

$$d\rho^{iTF}\left(V\right) = \frac{V^{T}\rho^{iT} + dV\sum_{j}\alpha_{ij}\rho^{jP}}{V^{T} + dV}. \tag{4.7}$$

In this chapter, the matrix α includes an additional row in order to account for dislocation transmutation into sessile, higher order dislocations and equation 4.7 is modified in order to account for the dissociation of parent dislocations at twin grain boundaries. A normalized dissociation parameter η is introduced, representing the proportion of dislocation density that fails to transmute from the j^{th} slip system in the parent volume to the twin volume and does not contribute to density in the twin. This leads to the final, modified constitutive law

$$d\rho^{iTF}\left(V\right) = \frac{V^{T}\rho^{iT} + dV\sum_{j}\left(1-\eta_{j}\right)\alpha_{ij}\rho^{jP}}{V^{T} + dV}. \tag{4.8}$$

The model of [11] also contains constitutive laws for twin activation, propogation, and interaction. These remained unchanged in this chapter and are summarized in Appendix A.1.

4.3 Implementation and Calibration

The above described changes to the dislocation density model were implemented in the LANL code VPSC-7b by making changes directly to the subroutines UPDATE_CRSS_CG_disl and DATA_CRYS and were compiled using the GFortran GNU compiler. The model was calibrated using a three stage process. First, the values for α were assigned based on the correspondence method introduced by [14]. After this, values for the elements η_j were assigned, and finally, the slip and twinning parameters respectively associated with dislocation generation twin nucleation and propagation were adopted from [83].

4.3.1 Correspondence Method for Transmutation for the Construction of α

A generalized correspondence method for mapping a vector on a slip plane in a parent grain on to a corresponding slip plane inside a twin grain was first presented in the work of [14]. This method was further developed by [14] and applied by Neiwczas to twin modes in FCC [80] and HCP crystals [81]. Summarized in Chapter 2, the precise mathematical expression of the general theory of the correspondence method adapted by [81] in the case of Mg was adapted for the purpose of assigning values to the transmutation matrix α.

The onto mapping of slip systems in the parent volume to corresponding slip systems in the twin volume implemented by [81] provides explicite calculations for transmuting the plane normal and directional vectors for each slip system in a parent grain to its cor-

responding slip system inside a twin. Rather than using the method to calculate values of α at each deformation step, the transmutation matrix for $\langle 1\,0\,\overline{1}\,2\rangle$ twins was constructed in pre-processing. $\langle 1\,0\,\overline{1}\,1\rangle$ twins were not assumed to contribute to transmutation in this work as the onset of compression twinning in Mg is taking place at higher strains, and very closely associated with the nucleation of damage in the material, leading quickly to brittle failure. As such, the contributions of compression twins to dislocation transmutation were assumed to be negligable. Strictly for the purposes of the elementwise construction of α, the following assumptions were made:

1. The entirety of the dislocation density from a slip system in the volume fraction of the parent grain overtaken by a twin mode is considered to transmute to its corresponding slip system inside the twin grain. This pairing of slip systems is defined by the mappings defined by the correspondence method used by [81] for HCP materials.
2. The dislocation density of slip mode in the volume fraction of the parent grain overtaken by a twin volume is considered to be evenly distributed across the systems of that mode.
3. In this simulation, the dislocation density of any parent slip system corresponding to a slip system inside the twin grain that was not part of the prismatic, basal, or 2^{nd} order pyramidal $< c+a >$ slip modes was assumed to contribute to debris formation inside the twin as part of ρ_{deb}.

Working from these assumptions, the value of each element α_{ij} can be calculated as the proportion of systems from the j^{th} slip mode in the parent volume fraction which contribute to dislocation density in the i^{th} slip mode in twin volume fraction. This can be expressed as

$$\alpha_{ij} = \frac{n_j^C}{n_j^{tot}}, \tag{4.9}$$

where n_j^C is the number of slip systems in the j^{th} slip mode of parent volume mapped onto slip systems in the i^{th} slip mode inside the twin volume and n_j^{tot} is the total number of slip

systems in the j^{th} slip mode of the parent volume. The values of α_{ij} for Mg used in this work are summarized in Equation 4.10, with prismatic, basal, 2^{nd} order pyramidal ¡c+a¿ modes and debris corresponding to indices $1, 2, 3,$ and 4, respectively, as

$$\alpha = \begin{bmatrix} 0.0 & 0.333\bar{3} & 0.333\bar{3} \\ 0.333\bar{3} & 0.0 & 0.0 \\ 0.666\bar{6} & 0.0 & 0.0 \\ 0.0 & 0.666\bar{6} & 0.666\bar{6} \end{bmatrix}. \tag{4.10}$$

4.3.2 Parameters for Dissociation

The molecular dynamics simulations in the work of [53] suggest that the type of dislocation and its orientation relative to the advancing twin boundary play a significant role in determining whether a given dislocation will transmute across the boundary or dissociate upon contact. In the simulations presented in this work, screw type basal dislocations were allowed to transmute perfectly across tensile twin boundaries. Edge type dislocations would either transmute across these twin boundaries or dissociate into twinning disconnections according to their orientation relative to the twin boundary, with positively oriented dislocations transmuting across the boundary and negatively oriented ones dissociating.

The simulations presented in this work were conducted at relatively low strain regimes, with $\epsilon \leq 0.25$ for all simulations. As such, the following assumptions were made:

1. Dislocations from the prismatic, basal, and 2^{nd} order pyramidal $< c + a >$ modes are assumed to transmute.
2. The incidence of screw type dislocations at low strain regimes is quite low. As such, for the purposes of this work, it was assumed that the contributions to dislocation density inside the twin volume fractions made by these types of dislocations were negligible.

3. Relative to twin boundaries, it was assumed that dislocations with positive and negative Burgers vector occur in equal measure.

Accordingly, the proportion of dislocation density for each mode dissociated at twin boundaries rather than transmuted is set at

$$\eta_{prismatic} = \eta_{basal} = \eta_{pyramidal} = \eta_{higherorder} = 0.5. \tag{4.11}$$

4.3.2.1 Parameters for Dislocation Generation and Twin Nucleation and Propagation

Simulations from the work of [83] were taken as a baseline for the presented work, and parameters for the constitutive laws governing dislocation generation, drag stress, normalized activation energy, Hall-Petch effects, and critical stress values were taken from this work. Transmutation effects were used in place of twin storage factor, reducing the latter value to zero. The values of these parameters are summarized in Table 4.1.

Table 4.1: Parameters for hardening evolution of slip.

	Prismatic	Basal	Pyramidal$\langle c+a \rangle$
k_1 $^1/_m$	2.0E+9	0.25E+9	2.0E+9
$\dot{\epsilon}$ s^{-1}	1.0E+7	1.0E+7	1.0E+7
g^α	0.0035	0.0035	0.003
D_0^α MPa	3.4E+3	10.0E+3	0.08E+3
τ_0^α MPa	30	11	50
χ	0.9	0.9	0.9
HP^α	0	0	0
$HP^{\alpha\beta}$	0	0	0

Table 4.2: Parameters for hardening evolution of twinning.

	Tensil Twin	Compression Twin
τ_0^β MPa	$\tau_{crit} = 15, \tau_{prop} = 10$	$\tau_{crit} = 185, \tau_{prop} = 185$
HP^β	0	0
$HP_{TW}^{\beta\beta}$	0	0
$C^{\beta 1}$	0	0
$C^{\beta 2}$	0	0
$C^{\beta 3}$	0	0

4.3.3 Simulation

Experimental data from the work of [83] was utilized to establish a control data set where possible. In the case where such data were not available, comparisons were made to simulated results from the same work. In this work, rolled, pure magnesium with a highly basal texture in the normal direction was subjected to uniaxial compression along the normal and transverse directions, hereafter referred to as through thickness compression (TTC) and in-plane compression (IPC) directions, respectively. This was done in order to capture the anisotropic mechanical behavior of textured magnesium, and, in particular, to motivate both scant and profuse twin volume growth. Shown in Figure 4.1, the simulations presented in this work were performed along both TTC and IPC load paths on polycrystals consisting of 1944 grains with a highly basal texture in order to recreate the conditions under which the literature data was collected. The loading was conducted at room temperature conditions, with a strain increment of $\Delta\epsilon = 0.001$, up to a total compressive strain of $\epsilon = 0.25$.

4.4 Simulation Results

4.4.1 TTC Load Path

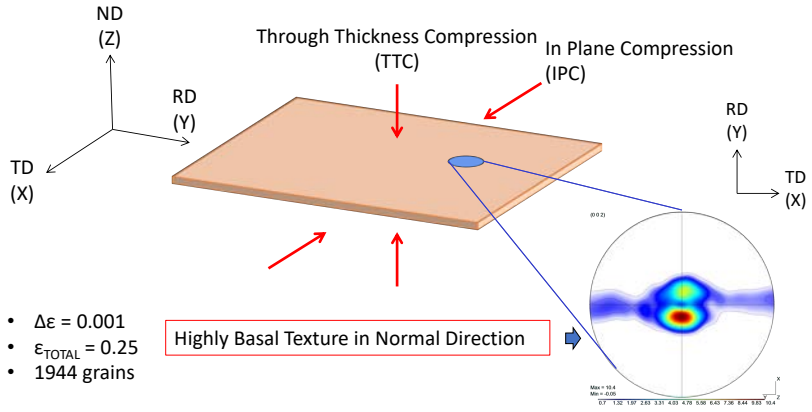

Figure 4.1: Simulated load paths and initial texture for simulations of rolled pure magnesium.

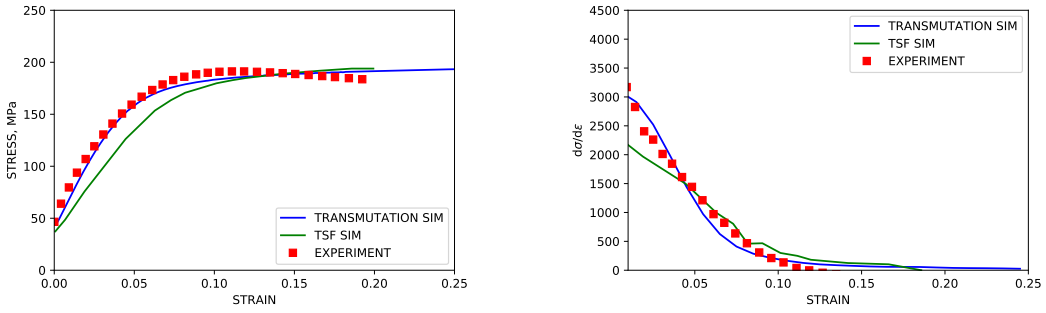

(a) (b)

Figure 4.2: Simulated and experimental mechanical response under TTC compression. (**a**) Stress-strain. (**b**) Hardening rate vs. strain.

As highlighted in figure 4.7, the TTC simulations reproduced both the texture and hardening curves from the experimental literature data with good accuracy. Although the strain softening observed in the experimental data at approximately $\epsilon = 0.1$ was not reproduced in the simulation, capturing such behavior lies beyond the scope of the current work. The simulated modal activity and evolution of twin volume fraction shown in Figure 4.3 both followed trends seen in simulations utilizing twin storage factor effects, though tension twin volume was somewhat under predicted relative to simulations utilizing the twin storage factor approach.

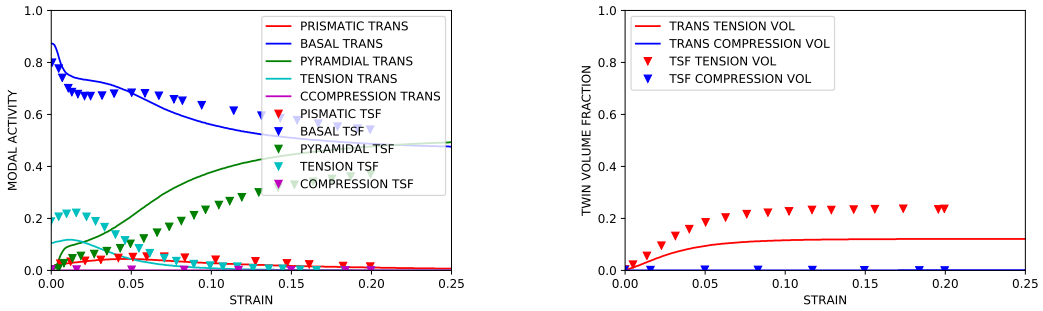

(a) (b)

Figure 4.3: Simulated slip and twinning activity under TTC compression compared to simulated results from [83]. (**a**) Simulated modal contributions vs. strain. (**b**) Simulated twin volume growth vs. strain

From the literature, the texture in TTC simulations was not expected to change much over the course of loading. This was evident in the simulations with the basal texture remaining consistent throughout the compression loading.

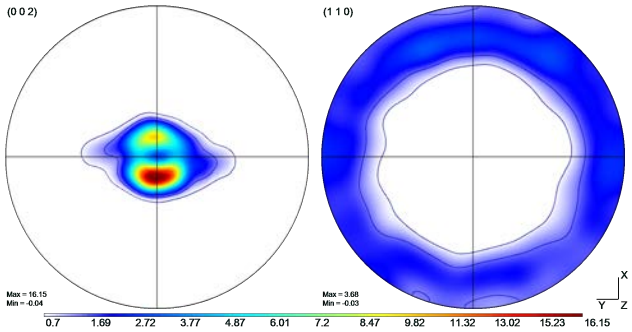

(a)

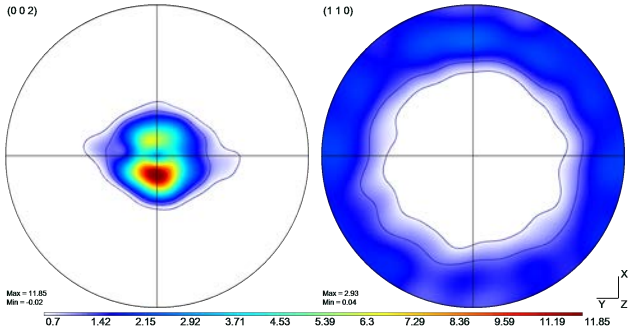

(b)

Figure 4.4: Comparison of simulated and experimental textures under TTC load conditions at ϵ=0.09 . (**a**) Simulated $(0\,0\,.\,1)$ and $(1\,1\,.\,0)$ pole figure. (**b**) Experimental $(0\,0\,.\,1)$ and $(1\,1\,.\,0)$ pole figures.

4.4.2 IPC Load Path

The sigmoidal stress curve associated with a high incidence of twinning was successfully captured in the IPC simulations. The associated simulated hardening rate was reasonably similar to experimental data from the literature. These results are shown in Figure 4.5. Modal contributions to strain were nearly identical to simulation results from previous simulation literature as well. The growth of secondary compression twin volume fraction did exceed that seen in simulations utilizing the twin storage factor approach, but it is assumed that this can be neglected as the onset of compression twinning is, at higher strains, associated with void nucleation along compression twin grain boundaries leading to brittle failure. This fact was reinforced by the failure of the experimental control specimen coinciding with the formation of significant ($> 10\%$) volume fraction of secondary compressive twins within the primary twin volume.

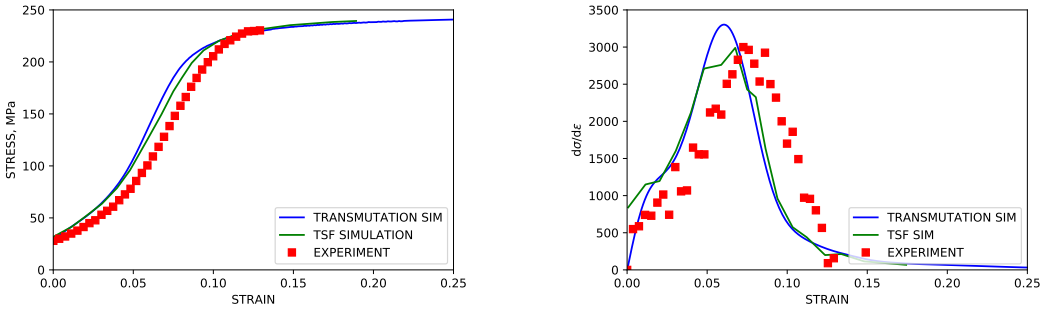

(a) (b)

Figure 4.5: Simulated and experimental mechanical response under IPC compression. (**a**) Stress -strain. (**b**) Hardening rate vs. strain.

Textural evolution was shown to be consistent with experimental data from the literature, with high concentrations of orientations in the neighborhood of 90°from the normal specimen axis. This type of reorientation is consistent with the high degree of tensile twinning.

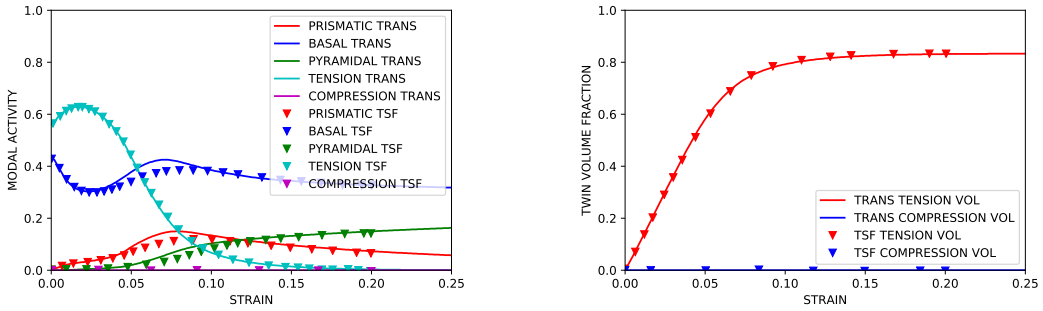

(a) (b)

Figure 4.6: Simulated parent slip and primary twinning activity under IPC compression compared to simulated results from [83]. (**a**) Simulated modal contributions vs. strain. (**b**) Simulated twin volume growth vs. strain.

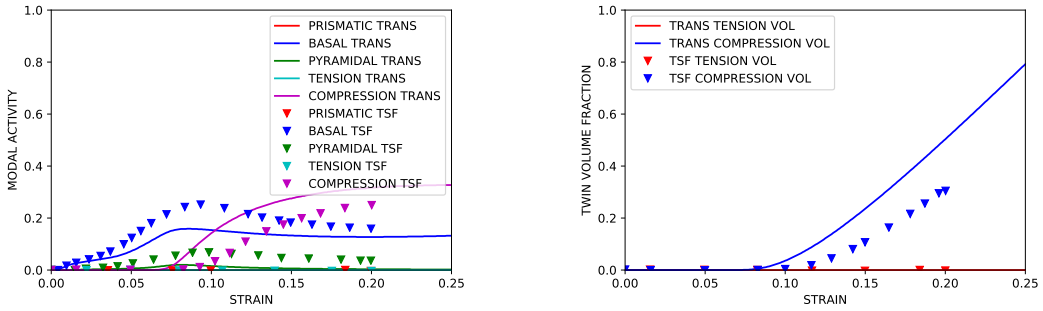

(a) (b)

Figure 4.7: Simulated twin slip and secondary twinning activity under IPC compression compared to simulated results from [83]. (**a**) Simulated modal contributions to strain vs. strain. (**b**) Simulated twin volume growth vs. strain.

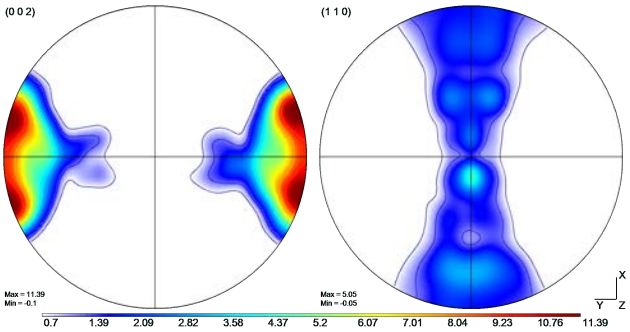

(a)

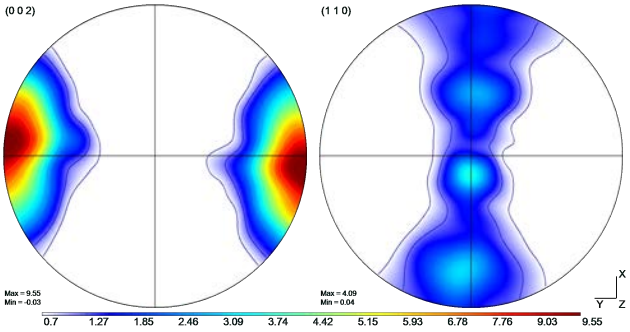

(b)

Figure 4.8: Texture comparison of simulated and experimental textures under IPC load conditions at ϵ=0.12 . (**a**) Simulated $(0\,0\,.\,1)$ and $(1\,1\,.\,0)$ pole figures. (**b**) Experimental $(0\,0\,.\,1)$ and $(1\,1\,.\,0)$ pole figures.

4.4.3 Comparison of Approaches

As the evolution of yield stress and twin volume with strain of pure magnesium is heavily anisotropic, it becomes necessary to consider a measure for "goodness of fit" of simulated data along multiple load paths when evaluating the degree to which the transmutation model and the method for calibrating its parameters are validated. This measure must also be extended to simulated data obtained from simulations utilizing the TSF model in order to make truly meaningful conclusions regarding connections between the mechanical behavior resulting from artificially increased dislocation density in twin grains and the increased dislocation density resulting from transmutation effects. To this end the normalized mean squared error (NMSE) was calculated across the simulated strain subdomains for which experimental data was available ($\epsilon = 0$ to 0.2 for TTC and $\epsilon = 0$ to 0.125 for IPC). Summarized in Table 4.3, these values were calculated for both load paths and for both modeling approaches.

Table 4.3: Normalized mean squared error for transmutation and TSF modeling approached.

	NMSE
Transmutation (TTC)	5.7613%
TSF (TTC)	$16.0268\ \%$
Transmutation (IPC)	21.0105%
TSF (IPC)	$16.7439\ \%$

For simulations of the TTC load path, the normalized mean squared error of the transmutation model is approximately 10% lower than that of the TSF model. In the IPC load path simulations, the normalized mean squared error is roughly 5% higher. Taking both of these comparisons into consideration, it can be concluded that while the transmutation model does suffer from some loss of accuracy in IPC simulations compared to the TSF approach, this loss is marginal at worst and more than offset by gains in accuracy in TTC simulations. This conclusion is further reinforced when one considers that the TSF model is a more empirical approach and, therefore, more limited than transmutation model by the availability of sound experimental data to insure its predictive capabilities.

4.4.4 η Sensitivity

Although stress-strain curves, texture evolution, and modal activities were consistent both with previous experimental and simulation work, further validation of the modeling approach is necessary to conclude that predicted results are indeed the product of increased dislocation density inside the twinned volume fraction of the simulated polycrystal.

In experiments and in simulations using both the TSF method and the method from the current work, the saturation stress observed in the TTC and IPC load paths differs significantly by approximately 60 MPa. In order to confirm that the "gulf" observed between the saturation stress levels of TTC and IPC simulations was in fact the result of increased hardness due to higher dislocation density brought on by dislocation transmutation, additional simulations in which transmutation effects were deactivated were performed for both load paths. This corresponds to simulations in which all of the dislocations dissociate

upon reaching the twin boundaries, leading to dissociation parameter values of $\eta = 1.0$. In these cases, the saturation stress levels for both TTC and IPC simulations were shown to be nearly equal, at roughly $\epsilon_{saturation} = 180$ MPa. These results are summarized in figure 4.9.

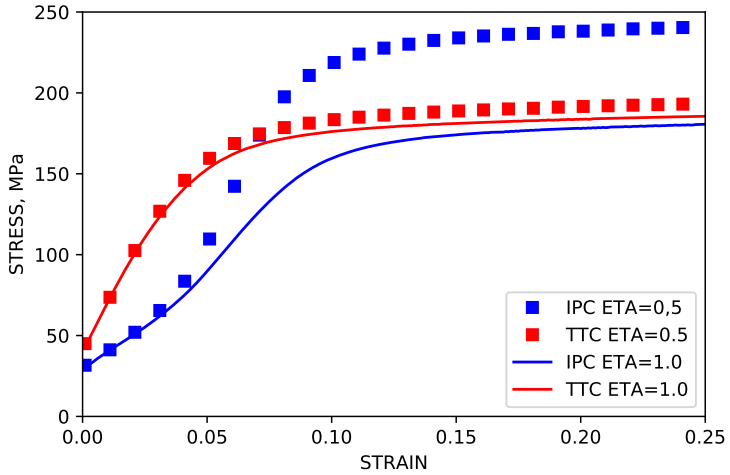

Figure 4.9: Simulated stress-strain curves with a dissocation parameter of η=0.5 and dissociation parameter η=1.0. These values correspond to a state of active dislocation transmutation and a state of no transmutation, respectively.

As shown in Figure 4.10b, the dislocation density evolution in IPC simulations is consistent with the simulations of [83]. The dislocation density of the twin volume fraction lies roughly in the range of twice that of the the dislocation density of the parent volume fraction.

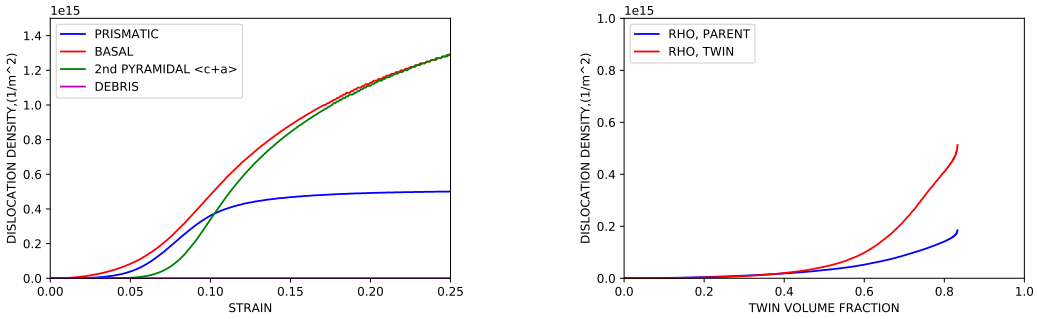

(a) (b)

Figure 4.10: Simulated dislocation density evolution. (**a**) Modal dislocation density vs. strain. (**b**) Dislocation density for parent and primary twin volume fractions vs. primary twin volume fraction.

The assumption that dislocations exist on the prismatic $\langle a \rangle$ and 2^{nd} order pyramidal $\langle c + a \rangle$ was also put to the test. IPC compression was simulated under the assumption that only basal dislocations would be allowed to transmute across twin grain boundaries. Shown in Figure 4.11, stress levels after the onset of twinning were noticably underpredicted. While stress levels for simulations with only basal dislocations actively transmuting were closer to approximating experimental stress levels than simulations in which no transmutation was activated, the relative similarities can be accounted for by acknowledging that deformation by basal slip, and therefore basal type dislocation density, is significantly higher than both prismatic $\langle a \rangle$ and 2^{nd} order pyramidal $\langle c + a \rangle$ in general. This is supported by observations of simulated dislocation density by mode, summarized in Figure 4.10a.

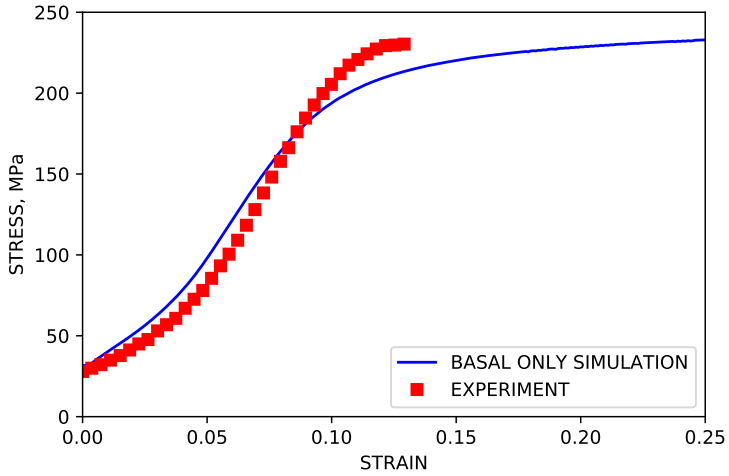

Figure 4.11: Simulated IPC stress curve with transmutation active in the basal mode only.

4.5 Analysis and Conclusions

In summary, methods for simulating the effects of twin transmutation and dissociation at twin grain boundaries was implemented in a visco-plastic self consistent framework in place of more conventional approaches that utilize Hall-Petch effects, and used to simulate uniaxial compression along multiple load paths in order to capture the behavior of magnesium under conditions which twin volume growth was both prefuse and sparse. The results of these simulations were compared to both experimental data and simulated data from previous approaches. The results permit highlighting the following points:

1. In place of Twin Storage Factor and Hall-Petch effects, a model for dislocation and twin boundary interactions was implemented. These methods and parameter selections were used to simulate the behavior of pure, basal textured, rolled magnesium subjected to uniaxial compression along (TTC) and perpendicular to (IPC) the dominant c-axis of the texture. The simulation results for stress, hardening, and texture development were consistent with observed experimental results. Modal activity and twin volume growth were largely similar to simulation work performed using the TSF approach.

2. The large difference between the saturation stress of the simulated IPC and TTC load paths was confirmed to be the result of transmutation effects included in the model by disabling the contributions of transmuted dislocations to the dislocation density of twin volume fractions.

3. It can be stated that Hall-Petch effects cannot be assumed to be the sole or even primary source of twinning induced anisotropy in the mechanical behavior of pure magnesium.

CHAPTER V

CONCLUSIONS

The work presented in this dissertation included the simulation of two twinning polycrystal materials, TWIP steels and pure magnesium, using self-consistent and, in the case of TWIP steels, fully constrained methods. These were done in order to investigate by simulation, the mechanical intersectionality of twin volume growth, textural development, grain boundary interactions, and mechanical hardening in heavily twinning materials.

In the first task, a method for the simultaneusly consideration of the growth multiple twin variants and their effects on texture evolution was developed and implemented in VPSC-7 and the self-consistent code developed at LEM3 at the Université de Lorraine. This twin volume transfer scheme was applied to simulations of hot rolled TWIP steel subjected to 90°ECAP on route Bc. Twin volume was controlled though the implementation of a disorientation driven attenuation in the consitutive function defining twin volume growth for each twin variant. In the case of the self-consistent code of LEM3, a Bronkhorst type hardening model was applied to capture the strain hardening behavior of the material. In VPSC-7, the Voce hardening law was applied with separate sets of hardening parameters assigned to parent and twin grains in order to capture mechanical behavior resulting from the interactions between parent grains and their relatively rigid twins. Simulation results

were generally consistent with experimental data with Taylor assumptions yielding the best results.

The interactions of slip dislocations with advancing twin grain boundaries and their effects on the strain hardening of pure magnesium were investigated in the second task. The dislocation density based hardening model of [11] was modified to consider the effects of dislocation transmutation across and dissociation at advancing twin grain boundaries on the mechanical hardening of rolled magnesium magnesium with a highly basal texture subjected to compression both parallel and perpendicular to the c-axis. This was done by incorporating a modified approach of [55] with the correspondence method developed by [14] and later adapted by [80] and [81] a dissociation parameter, η. Constants associated with transmutation and dissociation were assigned based on observations from molecular dynamics simulations of (cite El Kadiri and Barret) and the application of the correspondence method, and hardening parameters for the dislocation density based model were adopted from the work of [83]. All modeling parameters and constants were assigned *a priori*, without performing fitting to experimental data prior to simulation. The simulations yielded good agreement with both experimental data and previous simulation work without the need Hall-Petch effects.

5.1 Contributions

Recalling from the beginning of the dissertation, the aim of the work presented herein was to answer the following research questions:

1. To what extent does the simultaneous inclusion of the contributions of mulitple twin systems to textural evolution affect the ability to simulate and predict texture evolution in twinning polycrystals? Can these methods be used to supplement current approaches utilizing twin variant selection?
2. Does dislocation transmutation motivate hardening behavior in heavily twinning materials? If so, to what extent? Is there sufficient evidence to suspect that twin grain hardness due to transmutation effects acts as the primary driver of polycrystal materials in which it occurs or does it supplement Hall-Petch driven hardening?
3. What steps might be employed that reduce the reliance on empirically based methods used to "fit" modeling data to prexisting data?

Task 1 illustrated that methods based on a comprehensive view of all twin variants and their contributions to texture evolution can be used to predict texture evolution without the need for arbitrary twin variant selection criteria in the case of TWIP steel subjected to severe plastic deformation. By application of disorientation driven twin volume growth attenuation, the TVT scheme presented in this task also highlighted the need to consider the relative orientations of parent grains and their twins not just at the time of rerorientation, but also as the twins themselves develop into somewhat indpendent grains. The comparison of fully constrained to self-consistent approaches provided evidence that twinning microstructures in TWIP steel contribute to the enforcement of strain compatibility within a parent grain.

Task 2 showed that dislocation transmutation may have a substantial effect on the hardening behavior of polycrystal magnesium. Not only that, but transmutation may potentially inform the majority of hardening contributions associated with the incidence of twin boundary migration, thereby supplanting Hall-Petch type effects.

Taken together, the information gleaned from the results of both tasks suggest that substantial room lies open for improving the predictive capacity of current modeling ap-

proaches, specifically self-consistent methods, when applied to simulating the behavior of bulk material simply by more fully incorporating existing knowledge of lower length scale behaviors into the implemented constitutive relations. In doing so, it may be possible to reduce the reliance on emprically based fitting approaches thereby reducing the amount of time it takes to develop new simulations while simultaneously helping to better guide our understanding of the materials in question.

5.2 For Further Research

The methodology presented in Task 1 leaves open the possibility for continued refinement. At the time of writing, this method has only been applied to the problem of simulating the ECAP of TWIP steel, which is to say, it has only been tested on a narrowly defined strain regime when applied to a material with a high degree of symmetry and a very specific microstructural geometry. Validation of the model should continue at lower strain regimes and differing rates. Additionally, it becomes necessary to consider its application to twinning materials with lower crystal symmetries, specifically HCP materials like magnesium and titanium. Such simulations could certainly define the outer boundaries of the problem space of application as the twinning observed in these materials is likely to exhibit a radically different set of behaviors. How then, for instance, would twin volume growth attentuation play a role in grains where twin volume growth is dominated not by the nucleation of new twin grains as it is in TWIP steels, but by the migration of twin boundaries as it is in magnesium? In cases such as these, twin volume fraction rapidly overtakes

that of the parent grain, begging the question as to the validity of applying disorientation driven attenuation in such instances. This leads to further questions about what dislocation level characteristics give rise to grain boundary migration, or the lack thereof, in twinning materials?

For Task 2, one is forced to acknowledge the limiting nature of studies based purely on modeling and simulation methods, and so one is forced extend the work presented herein in an effort to further validate the findings. Two obvious methodological approaches for validation, both experimental and computational, present themselves at this time. Foremost among these approaches are experimental methods to verifying the differences in dislocation densities between twinned and untwinned regions of polycrystal magnesium. At present, the yet unpublished work of Zilahi, Toth, Ungar, and Ribarik developed a method for experimentally differentiating between twinned and untwinned volumes and calculating their respective dislocation densities using synchrotron measurements and applied it to calculating the dislocation densities twinned and untwinned grains of rolled AZ31. Once reviewed and published, this method represents a promising way to experimentally validate the current work. Until such time as this method becomes available for broader application, other experimental methods might be employed. Electron Channeling Contrast Imaging (ECCI) has been used to identify dislocation cells and mechanical twins in TWinning Induced Plasticity (TWIP) steals subject to tensile loading [38], and such an approach might be extended to magnesium. An observed build up of dislocation cells inside of observed twin grain boundaries would certainly support the findings of the presented work.

Extending the presented simulation approach to additional load paths and/or materials might provide limited validation as well; at the very least shedding some light on the bounds of predictive value that this model provides. Current limitations and foundational assumptions might not be sufficiently challenged in doing so, however, thereby calling into question the veracity of validation attempts based on such approaches. The substitution of known physical quantities for empirically fitted or assigned parameters in constitutive relations could support the findings of this work, however, as shrinking the ratio of empirically fitted parameters to experimentally observed values reduces the amount of uncertainty regarding the modeling approaches for the underlying physical phenomena. One such candidate for this tactic would be to adopt the approach for modeling the effects of self and latent hardening of Lavrentev [62]. By redefining the contributions of forest dislocations to CRSS in the context of the dislocation density based hardening model of [11] by using the shear modulus of the given mode, G, to the form

$$\tau^{\alpha}_{forest}\left(\rho^{\alpha}\right) = \mu \sum_{i} b^{\alpha}_{i} G_{i} \chi_{i} \sqrt{\rho^{\alpha}} \tag{5.1}$$

so as to differentiate the contributions of interactions across the combinations of paired slip modes $\alpha - i$, the single value of χ could be replaced with the values experimentally observed in [62].

The final, and likely most obvious avenue for further studies is the development of a comprehensive modeling approach that incorporates the approaches of both Task 1 and Task 2. The fact that brittle fracture is associated with the intersection of multiple tension twin grains in magnesium heavily suggests that any approach which considers more than

one twin variant could yield significant gains in predictive capability when information from mesoscale methods could be embedded in higher length scale continuum approaches for simulating components.

REFERENCES

[1] T. Al-Samman and X. Li, "Sheet texture modification in magnesium-based alloys by selective rare earth alloying," *Materials Science and Engineering: A*, vol. 528, no. 10-11, 2011, pp. 3809–3822.

[2] S. Allain, *Comportement mécanique des aciers : des mécanismes fondamentaux á la déformation macroscopique*, doctoral dissertation, Université de Lorraine, 2012.

[3] S. Allain, J. P. Chateau, O. Boaziz, S. Migot, and N. Guelton, "Correlations between the calculated stacking fault energy and the plasticity mechanisms in Fe–Mn–C alloys," *Materials Science and Engineering: A*, vol. 287-389, 2004, pp. 158–162.

[4] E. Bagherpour, M. Reihanian, and R. Ebrahimi, "On the Capability of Severe Plastic Deformation of Twining Induced Plasticity (TWIP) Steel," *Materials and Design (1980-2015)*, vol. 36, 2012, pp. 391–395.

[5] D. BARBIER, N. GEY, N. BOZZOLO, S. ALLAIN, and M. HUMBERT, "EBSD for analysing the twinning microstructure in fine-grained TWIP steels and its influence on work hardening," *Journal ofMicroscopy*, vol. 235, no. 1, October 2009, pp. 67–78.

[6] M. Barnett, "Twinning and the ductility of magnesium alloys Part II: "Contraction" twins," *Materials Science and Engineering: A*, vol. 464, 2007, pp. 8–16.

[7] M. Barnett, N. Stanford, P. Cizek, A. Beer, Z. Xuebin, and Z. Keshavarz, "Deformation Mechanisms in Mg Alloys and the Challenge of Extending Room-temperature Plasticity," *JOM*, vol. 61, no. 8, August 2009, pp. 19–24.

[8] C. Barrett and H. E. Kadiri, "The roles of grain boundary dislocations and disclinations in the nucleation of $\{10\bar{1}2\}$ twinning," *Acta Materialia*, vol. 63, 2014, pp. 1–15.

[9] Z. Basinski, M. Szczerba, M. Niewczas, J. Embury, and S. Basinski, "The transformation of slip dislocations during twinning of copper-aluminium alloy crystals," *Revue de Metallurgie, Cahiers d'Informations Techniques(France)*, vol. 94, no. 9, 1997, pp. 1037–1043.

[10] M. Berveiller and A. Zaoui, "An extension of the self-consistent scheme to plastically-flowing polycrystals," *Journal of the Mechanics and Physics of Solids*, vol. 26, no. 5-6, 1978, pp. 325–344.

[11] I. Beyerlein and C. Tomé, "A dislocation-based constitutive law for pure Zr including temperature effects," *International Journal of Plasticity*, vol. 24, no. 5, 2008, pp. 867–895.

[12] I. J. Beyerlein and C. N. Tomé, "A probabilistic twin nucleation model for HCP polycrystalline metals," *Proceedings of the Royal Society of London A: Mathematical, Physical and Engineering Sciences*, vol. 466, March 2010, pp. 2517–2544.

[13] B. Bhattacharya and M. Niewczas, "Work-hardening behavior of Mg single crystals oriented for basal slip," *Philosophical Magazine*, vol. 91, no. 17, June 2011, pp. 2227–2247.

[14] B. A. Bilby and A. G. Crocker, "The theory of the crystallography of deformation twinning," *Proceedings of the Royal Society of London A: Mathematical, Physical and Engineering Sciences*, vol. 288, no. 1413, 1965, pp. 240–255.

[15] J. Bishop and R. Hill, "XLVI. A theory of the plastic distortion of a polycrystalline aggregate under combined stresses.," *The London, Edinburgh, and Dublin Philosophical Magazine and Journal of Science*, vol. 42, no. 327, 1951, pp. 414–427.

[16] O. Boaziz, S. Allain, and C. Scott, "Effect of grain and twin boundaries on the hardening mechanisms of twinning-induced plasticity steels," *Scripta Materialia*, vol. 58, no. 6, 2008, pp. 484–487.

[17] O. Bouaziz, S. Allain, C. Scott, P. Cugy, and D. Barbier, "High manganese austenitic twinning induced plasticity steels: A review of the microstructure properties relationships," *Current Opinion in Solid State and Materials Science*, vol. 15, 2011, pp. 141–168.

[18] L. Bracke, K. Verbeken, L. Kestens, and J. Penning, "Microstructure and Texture Evolution During Cold Rolling and Annealing of a High Mn TWIP Steel," *Acta Materialia*, vol. 57, no. 5, 2009, pp. 1512–1524.

[19] C. Bronkhorst, S. Kalidindi, and L. Anand, "Polycrystalline plasticity and the evolution of crystallographic texture in FCC metals," *Philosophical Transactions of the Royal Society A*, vol. 341, 1992, pp. 341–443.

[20] U. Brüx, G. Frommeyer, O. Grässel, L. Meyer, and A. Weise, "Development and characterization of high strength impact resistant Fe-Mn-(Al-,Si) TRIP/TWIP steels," *Steel Research*, vol. 73, no. 6-7, June 2002, pp. 294–298.

[21] B. Budiansky and O. Mangasarian, "Plastic Stress Concentration at Circular Hole in Infinite Sheet Subjected to Equal Biaxial Tension," *Journal of Applied Mechanics*, vol. 27, 1960, pp. 59–64.

[22] E. C. Burke and W. R. H. Jr., "Plastic Deformation of Magnesium Single Crystals," *Journal of Metals*, vol. 295, 1952.

[23] C. Cáceres, P. Lukáč, and A. Blake, "Strain hardening due to 10 12 twinning in pure magnesium," *Philosophical Magazine*, vol. 88, no. 7, 2008, pp. 991–1003.

[24] M. Cherkaoui, "Constitutive equations for twinning and slip in low-stacking-fault-energy metals: a crystal plasticity-type model for moderate strains," *Philosophical Magazine*, vol. 83, no. 31-34, 2003, pp. 3945–3958.

[25] J. Christian and S. Mahajan, "DEFORMATION TWINNING," *Progress in Materials Science*, vol. 39, 1995, pp. 1–157.

[26] Y. CHUN and C. Davies, "Twinning-induced anomaly in the yield surface of highly textured Mg-3Al-1Zn plate," *Scripta Materialia*, vol. 64, 2011, pp. 958–961.

[27] M. Daamen, C. Haase, J. Dierdorf, D. A. Molodov, and G. Hirt, "Twin-roll strip casting: A competitive alternative for the production of high-manganese steels with advanced mechanical properties," *Materials Science and Engineering: A*, vol. 627, 2015, pp. 72–81.

[28] C. Davies and M. Barnett, "Expanding the extrusion limits of wrought magnesium alloys," *The Journal of The Minerals, Metals & Materials Society*, vol. 56, no. 5, 2004, pp. 22–24.

[29] U. Dehlinger, "Kristallplastizität mit besonderer Berücksichtigung der Metalle. Von Prof. Dr. E. Schmid und Dr.-Ing. W. Boas.(Struktur und Eigenschaften der Materie, Bd. XVII). Verlag von Julius Springer, Berlin 1935. IV und 373 S. 222 Abb. Preis geh. RM. 32,–, geb. RM. 33, 80," *Angewandte Chemie*, vol. 48, no. 30, 1935, pp. 518–519.

[30] J. Eshelby, "The determination of the elastic field of an ellipsoidal inclusion, and related problems," *Proceedings of the Royal Society of London A: Mathematical, Physical and Engineering Sciences*, vol. 241, no. 1226, 1957, pp. 376–396.

[31] T. Ezaza, M. D. Sangida, and H. Sehitoglua, "Energy barriers associated with slip-twin interactions," *Philosophical Magazine*, 2011.

[32] O. Grassel and G. Frommeyer, "High-strength and ultra-ductile FeMn (Al,Si) TRIP/TWIP light-weight steels for structural components in automotive engineering," *Stahl und Eisen*, vol. 122, no. 4, April 2002, pp. 65–69.

[33] O. Grässel, G. Frommeyer, C. Derder, and H. Hoffman, "Phase Transformations and Mechanical Properties of Fe-Mn-Si-Al TRIP-Steels," *Journal De Physique. IV*, vol. 07, no. C5, 1997, pp. C5–383–C5–388.

[34] O. Grässel, L. Krüger, G. Frommeyer, and L. W. Meyer, "High strength Fe–Mn–(Al, Si) TRIP/TWIP steels development — properties — application," *International Journal of Plasticity*, vol. 16, no. 10-11, 2000, pp. 1391–1409.

[35] C. Gu and L. Tóth, "Polycrystal modeling of tensile twinning in a Mg alloy during cyclic loading," *Scripta Materialia*, vol. 67, no. 7, 2012, pp. 673–676.

[36] C. Gu, L. Toth, and M. Hoffman, "Twinning effects in a polycrystalline magnesium alloy under cyclic deformation," *Acta Materialia*, vol. 62, 2014, pp. 212–224.

[37] I. Gutierrez-Urrutia and D. Raabe, "Dislocation and twin substructure evolution during strain hardening of an Fe–22wt.contrast imaging," *Acta Materialia*, vol. 59, no. 16, 2011, pp. 6449–6462.

[38] I. Gutierrez-Urrutia, S. Zaefferer, and D. Raabe, "Electron channeling contrast imaging of twins and dislocations in twinning-induced plasticity steels under controlled diffraction conditions in a scanning electron microscope," *Scripta Materialia*, vol. 61, 2009, pp. 737–740.

[39] C. HAASE, *Texture and microstructure evolution during deformation and annealing of high-manganese TWIP steels*, doctoral dissertation, RWTH Aachen University, 2016.

[40] C. Haase, L. A. Barrales-Mora, D. A. Molodov, and G. Gottstein, "Texture Evolution of a Cold-Rolled Fe-28Mn-0.28C TWIP Steel During Recrystallization," *Materials Science Forum*, vol. 753, 2013, pp. 213–216.

[41] C. Haase, L. A. Barrales-Mora, F. Roters, D. A. Molodov, and G. Gottstein, "Applying the Texture Analysis for Optimizing Thermomechanical Treatment of High Manganese Twinning-Induced Plasticity Steel," *Acta Materialia*, vol. 80, 2014, pp. 327–340.

[42] C. Haase, O. Kremer, W. Hu, T. Ingendahl, R. Lapovok, and D. A. Molodov, "Equal-channel angular pressing and annealing of a twinning-induced plasticity steel: Microstructure, texture, and mechanical properties," *Acta Materialia*, vol. 107, 2016, pp. 239–253.

[43] C. Haase, M. Kühback, L. A. Barrales-Mora, S. L. Wong, F. Roters, D. A. Molodov, and G. Gottstein, "Recrystallization Behavior of a High-Manganese Steel: Experiments and Simulations," *Acta Materialia*, vol. 100, 2015, pp. 155–168.

[44] C. Haase, C. Zehnder, T. Ingendahl, A. Bikar, F. Tang, B. Hallstedt, W. Hu, W. Bleck, and D. A. Molodov, "On the deformation behavior of -carbide-free and -carbide-containing high-Mn light-weight steel," *Acta Materialia*, vol. 122, 2017, pp. 332–343.

[45] E. Hall, "The deformation and ageing of mild steel: III discussion of results," *Proceedings of the Physical Society. Section B*, vol. 64, no. 9, 1951, p. 747.

[46] R. Hill, "Continuum micro-mechanics of elastoplastic polycrystals," *Journal of the Mechanics and Physics of Solids*, vol. 13, no. 2, 1965, pp. 89–101.

[47] P. B. HIRSCH and J. S. LALLY, "The Deformation of Magnesium Single Crystals," *Philosophical Magazine*, vol. 12, no. 117, May 1965, pp. 595–648.

[48] F. Hiura, R. K. Mishra, M. Lukitsch, and M. Niewczas, "NANO-INDENTATION STUDIES OF TWINNED MAGNESIUM SINGLE CRYSTALS," *Magnesium Technology*, 2012.

[49] P. V. Houtte, "Simulation of the rolling and shear texture of brass by the Taylor theory adapted for mechanical twinning," *Acta Metallurgica*, vol. 26, no. 4, 1978, pp. 591–604.

[50] P. V. Houtte, "Simulation of the rolling and shear texture of brass by the Taylor theory adapted for mechanical twinning," *Acta Metallurgica*, vol. 26, no. 4, 1978, pp. 591–604.

[51] W. Hutchinson and M. Barnett, "Effective values of critical resovled shear stress for slip in polycrystalline magnesium and other hcp metals," *Scripta Materialia*, vol. 63, 2010, pp. 737–740.

[52] J. J. Jonas, S. Mu, T. Al-Samman, G. Gottstein, L. Jiang, and E. Martin, "The role of strain accommodation during the variant selection of primary twins in magnesium," *Acta Materialia*, vol. 59, no. 5, 2011, pp. 2046–2056.

[53] H. E. Kadiri, C. Barrett, J. Wang, and C. Tomé, "Why are twins profuse in magnesium?," *Acta Materialia*, vol. 85, 2015, pp. 354–361.

[54] H. E. Kadiri, J. Kapil, A. Oppedal, L. Hector, S. Agnew, M. Cherkaoui, and S. Vogel, "The effect of twin–twin interactions on the nucleation and propagation of $\{1\,0\,\bar{1}\,2\}$ twinning in magnesium," *Acta Materialia*, vol. 61, no. 10, 2013, pp. 3549–3563.

[55] H. E. Kadiri and A. Oppedal, "A crystal plasticity theory for latent hardening by glide twinning through dislocation transmutation and twin accommodation effects," *Journal of the Mechanics and Physics of Solids*, vol. 58, no. 4, 2010, pp. 613–624.

[56] S. Kalidindi, C. Bronkhorst, and L. Anand, "Crystallographic texture evolution in bulk deformation processing of FCC metals," *Journal of Mechanics and Physics of Solids*, vol. 40, no. 3, 1992, pp. 537–569.

[57] S. R. Kalidindi, "Incorporation of deformation twinning in crystal plasticity models," *Journal of the Mechanics and Physics of Solids*, vol. 46, no. 2, 1998, pp. 267–290.

[58] E. Kröner, "Zur plastischen verformung des vielkristalls," *Acta metallurgica*, vol. 9, no. 2, 1961, pp. 155–161.

[59] A. Kumar, J. Wang, and C. Tomé, "First-principles study of energy and atomic solubility of twinning-associated boundaries in hexagonal metals," *Acta Materialia*, vol. 85, 2014, pp. 144–154.

[60] R. M. A. L. A. S. S. G. L. Jiang, J.J. Jonas, "Twinning and texture development in two Mg alloys subjected to loading along three different strain paths," *Acta Materialia*, vol. 55, no. 11, 2007, pp. 1359–6454.

[61] R. Lapovok, L. S. Tóth, A. Molinari, and Y. Estrin, "Strain localisation patterns under equal-channel angular pressing," *Journal of Mechanics and Physics of Solids*, vol. 57, no. 1, 2009, pp. 122–136.

[62] F. Lavrentev, "The type of dislocation interaction as the factor determining work hardening," *Materials Science and Engineering*, vol. 46, no. 2, December 1980, pp. 191–208.

[63] R. Lebensohn and C. Tomé, "A self-consistent anisotropic approach for the simulation of plastic deformation and texture development of polycrystals: application to zirconium alloys," *Acta metallurgica et materialia*, vol. 41, no. 9, 1993, pp. 2611–2624.

[64] R. Lebensohn and C. Tomé, "A self-consistent viscoplastic model: prediction of rolling textures of anisotropic polycrystals," *Materials Science and Engineering: A*, vol. 175, no. 1-2, 1994, pp. 71–82.

[65] R. Lebensohn, C. Tomé, and P. Maudlin, *An extended self-consistent viscoplastic formulation: application to polycrystals with voids*, Tech. Rep. LA-14044, Los Alamos National Lab (LANL), Los Alamos, NM (United States), August 2003.

[66] R. Lebensohn, C. Tomé, and P. Maudlin, "A selfconsistent formulation for the prediction of the anisotropic behavior of viscoplastic polycrystals with voids," *Journal of the Mechanics and Physics of Solids*, vol. 52, no. 2, 2004, pp. 249–278.

[67] R. Lebensohn, P. Turner, L. Signorelli, G. Canova, and C. Tomé, "Calculation of intergranular stresses based on a large-strain viscoplastic self-consistent polycrystal model," *Modelling and Simulation in Materials Science and Engineering*, vol. 6, no. 4, 1998, p. 447.

[68] X. Li, T. Al-Samman, S. Mu, and G. Gottstein, "Texture and microstructure development during hot deformation of ME20 magnesium alloy: Experiments and simulations," *Materials Science and Engineering: A*, vol. 528, no. 27, 2011, pp. 7915–7925.

[69] Y. Lü, B. Hutchinson, D. A. Molodov, and G. Gottstein, "Effect of Deformation and Annealing on the Formation and Reversion of -Martensite in an Fe–Mn–C Alloy," *Acta Materialia*, vol. 58, no. 8, 2010, pp. 3079–3090.

[70] Y. Lü, D. A. Molodov, and G. Gottstein, "Correlation Between Microstructure and Texture Development in a Cold-Rolled TWIP Steel," *ISIJ International*, vol. 51, no. 5, 2011, pp. 812–817.

[71] Y. Lü, D. A. Molodov, and G. Gottstein, "Recrystallization Kinetics and Microstructure Evolution During Annealing of a Cold-Rolled Fe–Mn–C Alloy," *Acta Materialia*, vol. 59, no. 8, 2011, pp. 3229–3243.

[72] E. Martin, L. Capolungo, L. Jiang, and J. Jonas, "Variant selection during secondary twinning in Mg–3*Acta Materialia*, vol. 58, 2010, pp. 3970–3983.

[73] R. Masson, M. Bornert, P. Suquet, and A. Zaoui, "An affine formulation for the prediction of the effective properties of nonlinear composites and polycrystals," *Journal of the Mechanics and Physics of Solids*, vol. 48, no. 6, 2000, pp. 1203–1227.

[74] M. S. Matoso, R. B. Figueiredo, M. Kawasaki, D. B. Santos, and T. G. Langdon, "Processing a Twinning-Induced Plasticity Steel by High-Pressure Torsion," *Scripta Materialia*, vol. 67, no. 7-8, 2012, pp. 649–652.

[75] H. Mecking and U. Kocks, "Kinetics of flow and strain-hardening," *Acta Materialia*, vol. 29, no. 11, 1981, pp. 1865–1875.

[76] A. Molinari, G. Canova, and S. Ahzi, "A self consistent approach of the large deformation polycrystal viscoplasticity," *Acta Metallurgica*, vol. 35, no. 12, 1987, pp. 2983–2994.

[77] A. Molinari and L. Tóth, "Tuning a self consistent viscoplastic model by finite element results—I. Modeling," *Acta Metallurgica et Materialia*, vol. 42, no. 7, 1994, pp. 2453–2458.

[78] X. M. M.R. Barnett, C.H.J. Davies, "An analytical constitutive law for twinning dominated flow in magnesium," *Scripta Materialia*, vol. 52, no. 7, 2005, pp. 627–632.

[79] T. Mura, *Micromechanics of defects in solids*, 2 edition, MARTINUS NIJHOFF PUBLISHERS, 1987.

[80] M. Niewczas, "Dislocations and twinning in face centred cubic crystals," *Dislocations in solids*, vol. 13, 2007, pp. 263–364.

[81] M. Niewczas, "Lattice correspondence during twinning in hexagonal close-packed crystals," *Acta Materialia*, vol. 58, no. 17, 2010, pp. 5848–5857.

[82] A. Oppedal, H. E. Kadiri, C. Tomé, S. Vogel, and M. Horstemeyer, "Anisotropy in hexagonal close-packed structures: improvements to crystal plasticity approaches applied to magnesium alloy," *Philosophical Magazine*, vol. 93, no. 35, 2013, pp. 4311–4330.

[83] A. L. Oppedal, H. E. Kadiri, C. N. Tomé, G. C. Kaschner, S. C. Vogel, and J. C. Baird, "Effect of dislocation transmutation on modeling hardening mechanisms by twinning in magnesium," *International Journal of Plasticity*, vol. 30-31, September 2012, pp. 41–61.

[84] P. Partridge and E. Roberts, "THE FORMATION AND BEHVAIOUR OF INCOHERENT TWIN BOUNDARIES IN HEXAGONAL METALS," *Acta Metallurgica*, vol. 12, 1964, pp. 1205–1210.

[85] N. Petch, "The cleavage strength of polycrystals," *J. Iron Steel Inst.*, vol. 174, 1953, pp. 25–28.

[86] G. Proust, C. Tom'e, and G. Kaschner, "Modeling texture, twinning and hardening evolution during deformation of hexagonal materials," *Acta Materialia*, vol. 55, no. 6, 2007, pp. 2137–2148.

[87] G. Proust, C. N. Tomé, A. Jain, and S. R. Agnew, "Modeling the effect of twinning and detwinning during strain-path changes of magnesium alloy AZ31," *International Journal of Plasticity*, vol. 25, no. 5, 2009, pp. 861–880.

[88] G. Sachs, "Plasticity problems in metals," *Transactions of the Faraday Society*, vol. 24, 1928, pp. 84–92.

[89] A. Saeed-Akbari, L. Mosecker, A. Schwedt, and W. Bleck, "Characterization and Prediction of Flow Behavior in High-Manganese Twinning Induced Plasticity Steels: Part I. Mechanism Maps and Work-Hardening Behavior," *Metallurgical and Materials Transactions*, vol. 43, no. 5, 2012, pp. 1688–1704.

[90] A. A. Saleh, C. Haase, E. V. Pereloma, D. A. Molodov, and A. A. Gazder, "On the evolution and modelling of brass-type texture in cold-rolled twinning-induced plasticity steel," *Acta Materialia*, vol. 70, 2014, pp. 259–271.

[91] A. A. Saleh, C. Haase, E. V. Pereloma, D. A. Molodov, and A. A. Gazder, "On the Evolution and Modelling of Brass-Type Texture in Cold-Rolled Twinning-Induced Plasticity Steel," *Acta Materialia*, vol. 70, 2014, pp. 259–271.

[92] A. A. Saleh, E. V. Pereloma, and A. A. Gazder, "Texture Evolution of Cold Rolled and Annealed Fe–24Mn–3Al–2Si–1Ni–0.06C TWIP Steel," *Materials Science and Engineering: A*, vol. 528, no. 13-14, 2011, pp. 4537–4549.

[93] A. A. Saleh, E. V. Pereloma, and A. A. Gazder, "Microstructure and Texture Evolution in a Twinning-Induced-Plasticity Steel During Uniaxial Tension," *Acta Materialia*, vol. 61, no. 7, 2013, pp. 2671–2691.

[94] I. Saxl, "The incorporation of slip dislocations in twins," *Czechoslovak Journal of Physics B*, vol. 18, no. 1, 1968, pp. 39–49.

[95] M. Shiekhelsouk, V. Favier, K. Inal, and M. Cherkaoui, "Modelling the behaviour of polycrystalline austenitic steel with twinning-induced plasticity effect," *International Journal of Plasticity*, vol. 25, 2007, pp. 105–133.

[96] S. Suwas, L. Toth, J. Fundenberger, T. Grosdidier, and W. Skrotzki, "Texture Evolution in FCC Metals during Equal Channel Angular Extrusion (ECAE) as a Function of Stacking Fault Energy," *Solid State Phenomena*, vol. 105, 2005, pp. 345–350.

[97] S. Suwas, L. S. Tóth, J.-J. Fundenberger, A. Eberhardt, and W. Skrotzki, "Evolution of Crystallographic Texture During Equal Channel Angular Extrusion of Silver," *Scripta Materialia*, vol. 49, no. 12, 2003, pp. 1203–6462.

[98] G. Taylor, "Plastic Strain in Metals," *J. Inst. Metals*, vol. 62, 1938, p. 307.

[99] I. Timokhina, A. Medvedev, and R. Lapovok, "Severe Plastic Deformation of a TWIP Steel," *Materials Science and Engineering: A*, vol. 593, 20214, pp. 163–169.

[100] C. Tomé, R. Lebensohn, and U. Kocks, "A model for texture development dominated by deformation twinning: application to zirconium alloys," *Acta Metallurgica et Materialia*, vol. 39, no. 11, 1991, pp. 2667–2680.

[101] C. N. Tomé and R. A. Lebensohn, *Manual for Code: VISCO-PLASTIC SELF-CONSISTENT (VPSC), Version 7b*, Los Alamos National Laboratory.

[102] L. S. Toth, C. Haase, R. Allen, R. Lapovok, D. A. Molodov, M. Cherkaoui, and H. E. Kadiri, "Modeling the effect of primary and secondary twinning on texture evolution during severe plastic deformation of a twinning-induced plasticity steel.," *Materials*, vol. 11, no. 5, May 2018, p. 863.

[103] United States of America. National Science and Technology Council, *Materials Genome Initiative for Global Competitiveness*, 2011.

[104] S. Vercammen, B. Blanpain, B. D. Cooman, and P. Wollants, "Cold rolling behaviour of an austenitic Fe–30Mn–3Al–3Si TWIP-steel: the importance of deformation twinning," *Acta Materialia*, vol. 52, no. 7, 2004, pp. 2005–2012.

[105] H. Wang, N. Tao, and K. Lu, "Strengthening an Austenitic Fe–Mn Steel Using Nanotwinned Austenitic Grains," *Acta Materialia*, vol. 60, no. 9, 2012, pp. 4027–4040.

[106] H. Wang, P. Wu, C. Tomé, and J. Wang, "A consitutive model of twinning and detwinning for hexagonal close packed polycrystals," *Materials Science and Engineering: A*, vol. 555, 2012, pp. 93–98.

[107] A. A. White, "Interdisciplinary collaboration, robust funding cited as key to success of Materials Genome Initiative program," *MRS Bulletin*, vol. 38, no. 11, 2013, pp. 894–896.

[108] www.worldautosteel.org, "Twinning-Induced Plasticity (TWIP) Steel Twinning-Induced Plasticity (TWIP) Steel,", July 17, 2018.

[109] Z. Yanushkevich, A. Belyakov, C. Haase, D. Molodov, and R. Kaibyshev, "Structural/textural changes and strengthening of an advanced high-Mn steel subjected to cold rolling,," *Materials Science and Engineering: A*, vol. 651, 2016, pp. 763–773.

[110] Y. Zhou, K. Neale, and L. T'oth, "A modified model for simulating latent hardening during the plastic deformation of rate-dependent FCC polycrystals," *International Journal of Plasticity*, vol. 9, no. 8, 1993, pp. 961–978.

APPENDIX A

APPENDIX

A.1 Parameters for Dislocation Density Based Hardening

Constitutive equations for twin hardening evolution in [11]:

$$\tau_c^t = \tau_0^k + \tau_{HP}^t + \tau_{slip}^k \tag{A.1}$$

$$\tau_{HP}^t = \begin{cases} \dfrac{HP^k}{\sqrt{d_g}} \text{ no twinning or when } t = \text{predominate twin system,} \\ \dfrac{HP^{kk'}}{\sqrt{d_{mfp}^s}}, \text{ when } t \neq \text{predominate twin system.} \end{cases} \tag{A.2}$$

$$\tau_{slip}^k = \mu \sum_i C^{ik} b^k b^i \rho^i \tag{A.3}$$

Table A.1: Parameters for hardening evolution of twinning.

	Tensile Twin	Compression Twin
τ_0^β MPa	$\tau_{crit} = 15, \tau_{prop} = 10$	$\tau_{crit} = 185, \tau_{prop} = 185$
HP^β	0	0
$HP_{TW}^{\beta\beta}$	0	0
$C^{\beta 1}$	0	0
$C^{\beta 2}$	0	0
$C^{\beta 3}$	0	0